2021-12-02

Chemical and Physical Weathering Rates of Basaltic Volcanic Regions: Utilizing Space in Place of Time in the Hawaiian Archipelago

Benjamin Clyde Barton
Brigham Young University

Chemical and Physical Weathering Rates of Basaltic Volcanic Regions:

Utilizing Space in Place of Time in the Hawaiian Archipelago

Benjamin Clyde Barton

A thesis submitted to the faculty of
Brigham Young University
in partial fulfillment of the requirements for the degree of

Master of Science

Stephen T. Nelson, Chair
Barry R. Bickmore
John Henry McBride

Department of Geological Sciences

Brigham Young University

ABSTRACT

Chemical and Physical Weathering Rates of Basaltic Volcanic Regions:
Utilizing Space in Place of Time in the Hawaiian Archipelago

Benjamin Clyde Barton
Department of Geological Sciences, BYU
Master of Science

With large populations living in tropical regions of the world with volcanic substrates, understanding basalt weathering processes is vital. The Hawaiian Islands are an excellent natural analogue to study chemical weathering rates due to a uniform bedrock (basalt), large variations in rainfall, and varying ages across the islands. Laterite weathering profiles (LWP) develop through chemical weathering, where LWP thickness is influenced by many factors, including precipitation and time.

Using the rapid, non-invasive horizontal-to-vertical spectral ratio (HVSR) method, LWP thicknesses can be estimated to constrain chemical weathering rates. Studying the laterite weathering profiles developed from basaltic bedrock of varying ages on Oahu (~2 Ma), Molokai (~1 Ma) and Kohala, Hawaii (~0.3 Ma) reveals three profiles in varying developmental stages. Over 200 HVSR soundings were collected on Oahu, Molokai, and Kohala. Shear wave velocity values of LWPs were determined by MASW (multichannel analysis of surface waves), and LWP thicknesses were verified from geologic logs and outcrop.

Oahu has thick LWPs compared to the other islands and shows a trend of increasing thickness with increasing precipitation across the island. The Molokai LWP follows a trend similar to Oahu, with a noticeable difference of thicknesses (20-40 m) at similar precipitation thresholds. Molokai presented a unique case, where the shear-wave velocity (V_s) boundaries between laterite and basalt were gradational for ~43% of HVSR datapoints, resulting in featureless frequency spectra that could not reliably model laterite-basalt boundary depths. The gradational nature of the LWP of Molokai is attributed to the young age of the island, and primary permeability properties of the thick, post-shield alkalic lavas. Molokai has an aerially average weathering rate of 0.02 to 0.04 m/ka. Kohala HVSR data show a newly developed LWP with varying LWP thickness within the same precipitation isohyet. LWPs on Kohala show a unique trend where LWP is thickest along the coast and is wedge shaped thinning out towards higher elevations. Each island differs in age and has its own unique LWP trends, with older islands tending to have deeper, more developed LWPs at similar precipitation ranges.

Keywords: Molokai, Hawaii, erosion rates, weathering reactions, laterite thickness, HVSR

ACKNOWLEDGMENTS

This thesis project wouldn't have been possible without the support and funding from the Geology Department at Brigham Young University and all the effort and time invested by the committee chair, Dr. Stephen Nelson, and committee members, Dr. Barry Bickmore and Dr. John McBride. Thanks goes to Kevin Ray and Eugene Wolfe for all the help provided in Hawaii and to all the undergraduates who helped with the HVSR instruments across the islands.

Thanks to my parents, for all their encouragement during my undergraduate and graduate studies, and especially their patience with me and my many rocks around their house. I thank my wife, Katie, who has never given up on me and has helped me immensely with the long days and nights involved in obtaining a master's degree.

TABLE OF CONTENTS

LIST OF FIGURES

LIST OF TABLES

1. INTRODUCTION

Hawaii experiences varying intensities and volumes of precipitation (Fig. 1) making it an environment conducive to development of thick and dynamic laterite weathering profiles (LWP) (Lau and Mink, 2006). The Hawaiian Island chain also consists of islands of varying ages; thus, the development and maturation of LWPs through time can be seen across the islands.

The purpose of this study is to evaluate the erosion rates of various Hawaiian Islands through the analysis of LWPs and precipitation trends through time. These islands lose mass by physical erosion and chemical erosion through streams and leaching of bedrock during the weathering process. A combination of water budget data and solute flux analysis determines the weathering rate from both physical erosion and leaching (Nelson *et al.,* 2013; Tolworthy, 2020). Analyzing the relationship between precipitation gradients, LWPs, and age across several islands provide insight on the developmental trends of LWPs through time.

1.1 Description of Study Areas

Starting about 5.1 Ma, the large islands of the Hawaiian Archipelago, a segment of the Hawaiian Seamount Chain, began forming above a stationary hotspot underneath the moving Pacific plate (Sherrod *et al.,* 2007). The Pacific plate moves in a northwest absolute direction; thus, the islands decrease in age to the southeast (Sherrod *et al.*, 2007). Rainfall across the islands varies greatly, with higher precipitation on the windward side (Fig. 1). The details of volcanic substrate composition can vary from island to island, but overall, the islands have a primarily tholeiitic basalt composition with some minor alkaline rocks (Sherrod *et al.,* 2007). This study focuses on three islands: Oahu, Molokai, and Hawaii.

1.1.1 Oahu

Oahu volcanism has ages of 0.04–4.0 Ma and is comprised of two extinct volcanic mountain ranges. The Ko'olau range (1.78–3.0 Ma) makes up the eastern part of the island and the Waianae range (2.9–4.0 Ma) comprises the western part (Sherrod *et al.,* 2007; Stearns *et al.,* 1935). Two volcanic stages are associated with the Ko'olau Range: the Ko'olau basaltic shield-forming stage volcanism and the much younger Honolulu rejuvenation-stage alkalic volcanism (0.04–0.1 Ma) (Sherrod *et al.,* 2007; Stearns *et al.,* 1935).

1.1.2 Molokai

Molokai volcanism has ages of 1.2–2 Ma and is comprised of two volcanic mountain ranges, East Molokai and West Molokai (Beeson 1976, Sherrod *et al.,* 2007). East Molokai volcanic stratigraphy is split into two members with the upper member consisting of andesites and trachytes and the lower member consisting of basalts (Stearns *et al.,* 1947). Sherrod *et al.,* (2007) records the lower member containing tholeiitic, transitional, and alkalic basalts.

1.1.3 Hawaii

Hawaii is still experiencing active volcanism. However, the extinct Kohala shield volcano includes exposed lavas that are as old as 0.78 Ma but are more commonly around 0.303–0.35 Ma (Chadwick *et al.,* 2003; Wolfe *et al.,* 1996; Sowards *et al.,* 2017; Sherrod *et al.,* 2007; Stearns *et al.*, 1946). The Kohala peninsula is the chief location on the island to have developed a substantial lateritic weathering profile.

Volcanic deposits that make up the Kohala Mountain are from the Hawi and Polulu volcanic eruptions, with the Hawi lava flows being more recent, ranging in age from 0.35–0.11 Ma. (Chadwick *et al.,* 2003; Sherrod *et al.,* 2007). Wolf *et al.,* (1996) classified the Polulu volcanic flow composition as basalt, whereas the Hawi volcanic basalt composition ranges from hawaiite to mugearite and benmoreite.

2. METHODS

2.1 Field Methods

Horizontal Vertical Spectral Ratio (HVSR) soundings were collected on the three islands (Tables 1–3). The locations for each survey were restricted to accessible areas such as parks, trails, or where safe, the shoulder of public roads (Fig. 2–4). HVSR soundings were recorded using 3-component Tromino ENGY 3G seismometers at a sampling rate of 128 Hz for twenty-minutes. The seismometer was leveled and coupled to the ground with a northward orientation on steel spikes attached to the base of the unit. Each site had a mixture of anthropogenic and natural source vibrations. Most common vibration sources were foot and vehicle traffic, ocean waves striking the island, and vegetation agitated by the trade winds. The seismometers were placed to avoid direct contact with any loose vegetation that could interfere with recording due to wind.

HVSR seismic soundings measure spectral amplifications between 0.1 and 64 Hz (Castellaro *et al.,* 2005). These measurements were analyzed and modeled with the Grilla software package using default settings to filter out excess noise within each sounding (Castellaro *et al.,* 2005). Within Grilla's software, several modeling variables can be held constant through the modeling process due to the relatively homogenous chemical composition of basalt across the islands (Fig. 5). Although the Grilla modeling is more or less insensitive to Poisson's ratio, values used for Poisson's ratio were set at 0.45 for laterite and 0.25 for basalt (Nelson *et al.,* 2019). These values are within an acceptable range on the high plasticity index for clay-rich rocks (Look, 2004). Density was held at 1.1 g/cm^3 for topsoil, 1.3 g/cm^3 for laterite, and 2.6 g/cm^3 for basalt following the procedures of Nelson *et al.* (2020) and based on guidance from published values by Porder *et al.* (2007). Laterite shear-wave velocity (V_s) was held at 300 m/s as

suggested by Nelson and McBride (2019) for saprolites developed over basalt (Yaede *et al.*, 2015; Nelson *et al.,* 2020). Modeled basalt V_s ranged from 450 m/s–650 m/s, which is comparable to the range reported by Wong *et al.* (2011) of 276 m/s–582 m/s. Greater detail for HVSR modeling parameters and procedures is provided in Nelson *et al.* (2020).

With the previously mentioned variables held constant, the data were analyzed using a two-layer forward modeling technique as used by Nelson and McBride (2019). This technique uses the fundamental mode equation (Eq 1) with a 2-layer model (laterite upper layer over an infinite half space of basalt bedrock) to estimate depth of the laterite-bedrock boundary. Specifically, one alters laterite-basalt depth until the model provides a good fit for the spectrum (Fig. 5).

Eq 1) $$f_o = \frac{V_s}{4d}$$

f_o = Resonant Frequency

V_s = Shear Wave Velocity

d = Depth of Velocity Boundary

After obtaining and modeling the HVSR spectra, the soundings were categorized qualitatively as 1, 2, or 3 (Fig. 6 & Tables 1–3). Spectra assigned #1 are flat, attributed as the result of gradational weathering boundaries, and resulted in no model. Spectra categorized #3 have clearly distinct peaks allowing the model to have a good fit with a high degree of confidence. Spectra assigned #2 have low-amplitude peaks with soft shoulders that are sometimes not distinct enough from the surrounding spectrum to be entirely unambiguous. Datapoints in this category were analyzed one at time with all points categorized as quality #3 to determine an overall trend for the island. If the point was an extreme outlier, it was changed to category 1, no model.

Due to the lack of information regarding Molokai's soil and seismic physical characteristics, several 1-dimensional MASW seismic surveys were conducted, and 25 soil samples collected (Fig. 3). Soil sample and survey collection was not needed for Oahu or Hawaii due to soil mineralogy and chemistry being widely documented and published for those islands (Chadwick *et al.,* 2003; Goodfellow *et al.,* 2014; Nelson *et al.,* 2013; Porder *et al.,* 2007; Sowards *et al.,* 2017; Wong *et al.,* 2011). Each Molokai sample was collected from exposed surface soil and stored in sterile 50 ml tubes before being sent to Brigham Young University (BYU) for analysis. MASW data acquisition parameters were similar to those used by Yaede *et al.* (2015). MASW field parameters include source and receiver spacings of 3.048 m, with 24 in-line geophones. In addition to active surveys, "passive" surveys that mimic dynamic roadside surveys were conducted by striking the aluminum plate at approximately 2-second intervals and at a constant source receiver offset of 3.048 m. These surveys help constrain the interpretation and modeling of HVSR spectra by providing some of the variables used in the fundamental mode equation and by providing a comparison of laterite depths in regions where both types of surveys were taken.

2.2 Terrain Modeling Methods

Field conditions do not always allow readings to be taken on ridgelines or local topographic highs, representing the least eroded features in the surrounding topography. To account for any recent erosion and obtain as true laterite thickness as possible, laterite depth corrections were performed using terrain analysis modeling (TAM) within ArcGIS Pro, following similar procedures in the modeling technique used by Ferrier *et al.,* (2013) and Gayer *et al.,* (2019). Digital elevation model (DEM) data obtained from the National Map Data Downloader (USGS, 2021) for each island was imported into ArcGIS Pro. Ridgelines were

digitized along interfluvial ridges in the study areas and the *extract value to point* tool used to assign elevation data to these points. The *inverse distance weighted* (IDW) tool created a raster of the estimated pre-erosional surface elevation. HVSR sounding point elevations were subtracted from the pre-erosional raster elevation. Sounding points with a negative value were corrected by adding in the difference in elevation to represent the original lava depositional elevation.

There will always be some error involved with this method of calculating physical erosion due to the manually input ridgeline points used to create the pre-erosional surface raster. It is important to note that due to the relatively young age of the Kohala, no erosion correction is needed for the LWP data points on Kohala.

2.3 Laboratory Methods

The soil samples were prepared at BYU for analysis by X-ray fluorescence (XRF) and X-ray diffraction (XRD). Samples were first air dried in a HEPA (high efficiency particulate air) hood for over 24 hours. Sample preparation and analysis then followed the same whole-rock chemical analysis procedures outlined in Dailey (2016) for XRF analysis. Due to an abundance of residual water within the clays and a high concentration of organic components preventing the instruments from functioning properly, soil samples were first calcined through a 2-stage loss on ignition (LOI) procedure before glass disk and pellet creation. First stage LOI was run at 400 °C for 2 hours with second stage at 1000 °C for 2 hours. Water and organic matter mass were factored back into the results post LOI analysis.

2.3.1 Tau Values

To determine the extent and quantity of solutes mobilized within the weathered soil, major and trace elemental compositions of bedrock protoliths (Beason 1976, Clague and Moore,

2001) were compared with the 25 soil samples collected on Molokai to determine Tau (τ) values (Tables 4–5), calculated following Brantley and White's (2009) method (Eq 2). The immobile element used for major and trace element analysis is Ti. τ values are given as a percentage of leaching or accumulation, where negative values indicate leaching.

Eq 2) $$\tau = \left(\frac{C_{j,w} C_{i,p}}{C_{j,p} C_{i,w}} - 1 \right) \times 100$$

$C_{j,w}$ = concentration of element *j* within weathered soil

$C_{j,p}$= concentration of element *j* within unweathered protolith soil

$C_{i,w}$= concentration of immobile element *i* within weathered soil

$C_{i,p}$= concentration of element *i* within unweathered protolith soil

2.3.2 Weathering Reactions

Weathering reactions were created to show the transfer of material during chemical weathering. The composition of product minerals in the weathering reactions was determined from XRD analysis of the soil samples (Nelson, 2013). Reactant mineral compositions were estimated through the MELTS program (Ghiorso and Sack, 1995, Asimow and Ghiorso, 1998). Initial lava composition was set as an average of the compositions listed in Beason (1976). MELT calculations were computed at 1 bar and 0 ΔQFM. The model ran until magma crystalized to 13%, similar to phenocryst concentrations in basalt on Molokai (Beason, 1976). MELT calculations for the groundmass started from a composition of parent rock subtracting phenocrysts composition and run until temperatures cooled to 745° C, when approximately 87% of liquid crystalized.

2.4 Water Budget

Spring and well groundwater data for Molokai Island were obtained from the National Water Information System (NWIS) (Table 6) (U.S. Geological Survey, 2016). Water data for the

study area on East Molokai volcano are extremely limited with no perennial streams present. A water budget for the study area on Molokai (Fig. 7), used to evaluate erosion by groundwater seepage, was calculated using ArcGIS Pro (Giambelluca *et al.,* 2013). Annual precipitation and annual evapotranspiration raster data used in the budget was obtained from the Rainfall Atlas of Hawaii (Frazier *et al.,* 2016) published online through the University of Hawaii (Giambelluca *et al.,* 2013). A simplified water budget is:

Eq 3) $$P = ET + GW$$

$$P = precipitation$$

$$ET = evapotranspiration$$

$$GW = groundwater\ flux\ through\ the\ area$$

Detailed water budgets should also include a term for changes in soil moisture storage. However, over long time periods, these changes may be neglected (see references in Tolworthy *et al.,* 2020). Due to the homogeneous nature of the volcanic bedrock on East Molokai volcano, it was assumed that groundwater chemistry is homogeneous throughout the study area. A published water budget from Shade (1997) was used for calculations involving the entire island of Molokai. Solute flux was calculated for the study area in Molokai in a fashion similar to Nelson *et al.* (2013) by multiplying the total dissolved solute concentration by groundwater flux.

3. RESULTS

3.1 Oahu

Data was collected on Oahu in localized groups cutting across rainfall isohyets. From north to south, the groups consist of Pupukea, Poamoho, ‘Aeia heights, and Tantalus Drive (Fig. 2 & 8). A total of 99 HVSR soundings were recorded on Oahu (Fig. 2) with 30 points that could not be modeled due to either equipment failure or classification as quality category 1 (Table 2).

Erosion-corrected laterite depths on Oahu ranged from 6 to 96 m with an average depth of 53 m (Fig. 8). No soil samples or MASW surveys were collected on Oahu, due to this information previously being published (Yaede *et al.,* 2015; Nelson *et al.,* 2013; Nelson and McBride, 2019)

3.2 Molokai

For the purpose of this study, particular attention was placed on a 14.1 x 10^7 m^2 rectangular area on the west flank of East Molokai volcano (Fig. 3) where all 25 soil samples, several MASW surveys, and 63 seismic soundings were gathered along the Kamakou Forest Preserve Road. Of those 63 HVSR soundings, 27 were could not be modeled (Table 2). HVSR and soil sample collection began near Homelani Cemetery on the west end of the East Molokai Volcano and ended just below the summit at Pepeopae Trail Head. Precipitation isohyets ranged 500–3000 mm/yr within the zone of interest. Erosion-corrected laterite thickness in the study area ranged from 7 to 71 m, with an average thickness of 36 m (Fig. 9).

3.3 Kohala, Hawaii

A total of 71 HVSR soundings were recorded on Kohala (Fig. 4) with 20 points that could not be modeled due to either equipment failure or classification as quality category 1. Within the Kohala peninsula, laterite depth ranged from 1 to 28 m, with an average depth of 8 m (Fig. 10). 46 HVSR soundings were recorded on the Pololu volcanic substrate, with 5 soundings taken on the younger Hawi basalt. 48 HVSR seismic soundings were collected between the 1500 and 2000 mm/yr isohyets with 3 soundings recorded in the 1000–1500 mm/yr range. No soil samples or MASW surveys were collected on Kohala, with this information previously being published (Chadwick *et al.,* 2002; Sowards *et al.,* 2017; Porder *et al,* 2007; Nelson *et al.,* 2020; Nelson and McBride, 2019).

Soil pits dug by Porder *et al.,* (2007) show the laterite profiles are thin (<5m), however the northern tip of the peninsula has laterite thicknesses of up to 40 m (Goodfellow *et al.,* 2014; Sowards *et al.,* 2018). The windward side of the northern tip on Kohala contains some of the island's deeper weathering profiles due to the accumulation of groundwater near the coast, precipitation, and the large volume of organic material in the soil (Sowards *et al.,* 2018; Porder *et al.,* 2007; Nelson *et al.,* 2020).

4. DISCUSSION

4.1 Laterite thickness as a function of precipitation and time

Analyzing precipitation trends vs. LWP depths reveal weathering trends of laterite in basaltic regions. Nelson *et al.* (2020) showed a linear correlation between laterite thickness and precipitation on Kauai and Oahu with a much more complicated relationship on young surfaces like Kohala. This study adds considerably to the available data in Nelson *et al.* (2020) for Oahu and allows insight to LWP development trends on Molokai. HVSR soundings across Oahu, Molokai, and Kohala have been analyzed in concert with precipitation data to show the evolution of laterites with both age and precipitation. The previously published relationship for Kauai in Nelson *et al.* 2020 is used to examine the trends across a greater time interval.

4.1.1 Oahu

Oahu is the oldest island of the three islands sampled. LWPs on older islands were expected to be more mature and have increasing laterite thicknesses from low to high precipitation thresholds with fully developed, clear, sharp V_s boundaries. HVSR data for most of Oahu supports this idea and shows a distinct cluster of thicker laterite profiles (50–96 m) with higher precipitation (1500–3000 mm/yr) commonly at higher elevations, and thinning laterite profiles (<5–50m) at lower elevations with lower precipitation (0–1500 mm/yr) (Fig. 8).

However, some of the data does not show this trend so clearly. This may be due to the late-stage rejuvenation volcanic eruptions within the last million years that formed some of the more publicly known volcanic vents and flows on southern Oahu, such as Diamond Head, Punchbowl Crater, and Koko Head (Sherrod *et al.,* 2007). The Tantalus Peak-Sugar Loaf vent system contains some of the youngest rejuvenated volcanic deposits with ages ranging from 0.1 to 0.04 Ma (Sherrod *et al.,* 2007). Due to the extremely young age of the rejuvenation basalts, the soundings collected along Tantalus drive in Southern Oahu do not follow the same trend as the rest of Oahu. Tantalus drive LWPs are shallow compared to LWP depths with the same precipitation thresholds as other areas on Oahu. When Tantalus Drive data is not included, HVSR data suggests a clear and consistent trend between LWP depths and annual rainfall (Fig. 8).

4.1.2 Molokai

Molokai yielded unexpected results from the HVSR surveys. The depth-to-precipitation trends were more difficult to interpret. As with the other islands surveyed, Molokai's HVSR soundings were expected to yield sharp seismic velocity boundaries for depths of precipitation levels similar to Oahu and Kohala. Spectra results were a mixture of sharp seismic velocity boundaries and relatively flat spectra with no velocity contrast peaks (Fig. 6). Featureless spectra have been more commonly observed on the leeward side of the island where there are lower annual precipitation rates, while the more mature LWPs (those with sharp boundary spectra) are observed on the windward side of the island with higher annual precipitation rates.

One possible explanation for the flat spectra could be the variation in permeability between post-shield alkalic lavas on Molokai and basalts on Kauai, Oahu, and Kohala (Nelson *et al.,* 2020; Sherod *et al.,* 2007). The post-shield lavas have varying weathering reaction rates

throughout the permeable saturation zone, causing a gradational change of seismic velocity boundaries within the laterite. Sowards *et al.* (2017) demonstrated that various phases of weathering can occur within a laterite profile through their investigation of a Kohala cliff face. Such gradational laterite zones can be recreated using a multi-layered model with increasing seismic velocity (Fig. 11). In a few cases on Molokai, MASW surveys show laterite velocity increasing incrementally in a step like pattern (Fig. 11)

With the gradational spectra removed, Molokai shows a strong linear relationship (r^2=0.9016) between precipitation and laterite depth, similar to trends on Oahu and Kauai (Fig. 12). At similar precipitation gradients, Molokai laterite thicknesses are on average shallower than those on Oahu, which are in turn shallower than those found on Kauai. Thus, it appears, with the passage of time, deeper LWPs develop when precipitation is held roughly the same.

4.1.3 Kohala Peninsula Hawaii

In addition to adding to the knowledge of the relationship between varying amounts of rainfall and laterite thickness on the Hawaiian Islands (Nelson *et al.,* 2020), this study includes an analysis of laterite thickness over an area with nearly constant rainfall. Most soundings collected in Kohala were recorded between the 1500 and 2000 mm/yr isohyets (Fig. 4). By eliminating precipitation as a variable, the relationship between laterite development and elevation can be better observed. A unique pattern was detected when looking at LWP depths within a set rainfall range (1500 to 2000 mm/yr), where laterite thickness decreases with an increase of elevation. Nelson *et al.* (2020) use differences in the vadose-zone hydrology to explain increased laterite thickness near the coast.

4.1.4 Summary of LWP thickness trends

The HVSR and MASW-derived laterite thicknesses show a strong relationship between higher volume of precipitation and increasing laterite thicknesses that is consistent across Kauai, Oahu, and Molokai (Fig. 12). This relationship is supported by the previously mentioned studies (Nelson *et al.,* 2020; Nelson and McBride, 2019; Porder *et al.,* 2007). Additionally, data from the younger island of Hawaii, suggests that elevation is a critical factor in laterite thickness when precipitation is roughly constant.

In addition to understanding the relationship between rainfall and thickness, the varying ages of Oahu, Molokai, and Hawaii provide greater insight on how age affects laterite thickness. For greater visual clarity, we fit a 3-dimensional model to the collective rainfall, laterite thickness, and age data (Fig. 13). The resulting curved plane represents the overall weathering trend for laterite in the Hawaiian Islands. Equation 4 is derived from the 3-D plot ($r^2 = 0.6182$).

Eq 4) $$T(\pm 31.2) = 3.4(\pm 1.5)A + 0.0068(\pm 0.0021)R + 0.0055(\pm 0.0018)AR$$

$$A = Basalt\ age\ (Ma)$$
$$R = Precipitation\ (mm/yr\ \ )$$
$$T = Laterite\ thickness\ (m)$$

It is important to note, this equation and model does not function well at low values of precipitation or age. Although the laterite thickness 95% confidence interval is relatively high (31 m), having a large dataset allows the overall weathering trend to be seen. A benefit from this model is the ability to predict how age, precipitation, and thickness influence each other. For example, constraining one variable (age, precipitation, thickness) within equation 4 results in an equation of a line, which can be used to provide trend information for the other two variables.

Thus, equation 4 may allow the estimation of laterite thickness of any tropical island with a basaltic bedrock, at a given age or rainfall above a certain threshold.

4.2 Mass Flux

While the bulk of this study focused on the relationship between laterite thickness and precipitation, it is important to understand how exactly basalt weathers to laterite and how mass is removed from the Hawaiian Islands. Mass flux values have previously been published for Kauai, Oahu, and Hawaii Islands (Tolworthy *et al.,* 2020; Nelson *et al.,* 2013; Nelson *et al.,* 2020; Porder *et al.,* 2007). This paper adds to existing research by reporting mass flux for Molokai, which is of intermediate age between Kohala (Hawaii) and Oahu.

4.2.1 Surface and Groundwater Flux

Although there is a published water budget for Molokai (Shade, 1997), a more specific water budget for the study area was calculated using data from the Hawaiian Rainfall Atlas (Frazier *et al.,* 2017) within ArcGIS. This water budget is split between 52% evapotranspiration and 48% groundwater recharge (Fig. 7). Using the USGS NWIS mapper, groundwater quality data was obtained from 10 groundwater or spring locations on the island (Table 6) (USGS, 2016). An average SiO_2 concentration from the 10 available groundwater data sources is 38.4 mg/L (U.S Geological Survey, 2016) leading to an aerially average weathering rate of 0.03– 0.06 m/ka. This rate is similar to the erosion rates of Oahu (0.004–0.041 m/ka), Kohala (0.013–0.047 m/ka), and Kauai (0.061 m/ka) (Nelson *et al.,* 2019; Toleworthy *et al.,* 2020).

4.2.2 Weathering Reactions

Laterite weathering profiles are the result of time and water-rock chemical reactions. The principal bedrock of Molokai is comprised of two basalt shield volcanoes (Sherrod *et al.,* 2007) resulting in a large amount of saprolite, clay and Fe-oxide rich soil overlying unaltered basalt

bedrock. XRD results (Table 7) show that soils along the forest preserve road in East Molokai contain primarily goethite, gibbsite, hematite, kaolinite, maghemite, quartz and a small percentage of other minerals.

Weathering reaction reactants were calculated by using XRF data with the MELTS program. The resulting weathering reactions are as follows:

Phenocryst Reactions

(1) Olivine Weathering $2\ (Mg89Fe11)2Si_{100}O_{400} + 197\ O_{200} + 796\ H_{100}^{+} \rightarrow 44\ Fe_2O_3 + 200\ H_4SiO_4 + 356\ Mg^{2+} + 394\ H_{200}O_{100}$

(2) Clinopyroxene Weathering $200\ NaCa_{82}Fe_{10}Mg_{94}Fe_3Ti_3Al_{21}Si1_{85}O_{600} + 70600\ H_{100} + 17477\ O_{200} \rightarrow 1300\ Fe_2O_3 + 32800\ SiO_2 + 2100\ Al_2Si_2O_5(OH)_4 + 1800\ Mg^{2+} + 16400\ Ca^{2+} + 200\ Na^{+} + 600\ TiO_2 + 35258\ H_{200}O_{100}$

(3) Feldspar Weathering $Na_{26}Ca_{74}Al_{174}Si_{226}O_{800} + 174\ H^{+} + 191\ H2O \rightarrow 87\ Al_2Si_2O_5(OH)_4 + 26\ Na^{+} + 74\ Ca^{2+} + 52\ H_4SiO_4$

Groundmass Reactions

(1) Feldspar Weathering $K_1Na_{47}Ca_{52}Al_{152}Si_{248}O_{800} + 268\ H_2O + 152\ H^{+} \rightarrow 76\ Al_2Si_2O_5(OH)_4 + 47\ Na^{+} + K^{+} + 52\ Ca^{2+} + 96\ H_4SiO_4$

(2) Feldspar Weathering $K_1Na_{47}Ca_{52}Al_{152}Si_{248}O_{800} + 152\ H_2O + 152\ H^{+} \rightarrow 152\ Al(OH)_3 + 47\ Na^{+} + K^{+} + 52\ Ca^{2+} + 248\ SiO_2$

(3) Clinopyroxene Weathering $4\ Na_2Ca_{88}Fe_{13}Mg_{90}Fe_1Ti_3Al_{13}Si_{191}O_{600} + 1432\ H^{+} + 15\ O_2 \rightarrow 28\ Fe_2O_3 + 712\ SiO_2 + 26\ Al_2Si_2O_5(OH)_4 + 360\ Mg^{2+} + 352\ Ca^{2+} + 8\ Na^{+} + 12\ TiO_2 + 664\ H_2O$

(4) Clinopyroxene Weathering $4\ Ca_9Fe_{42}Mg_{146}Al_5Si1_{97}O_6 + 1240\ H^{+} + 1227\ O_2 \rightarrow 84\ Fe_2O_3 + 768\ SiO_2 + 10\ Al_2Si_2O_5(OH)_4 + 584\ Mg^{2+} + 36\ Ca^{2+} + 600\ H_2O$

(5) Rhm-oxide Weathering $2\ Mn_7Fe_{55}Mg_{31}Fe_6Al_9Ti_{93}O_{300} + + 124\ H^{+} + 29\ O_2 \rightarrow 61\ Fe_2O_3 + 18\ Al(OH)_3 + 186\ TiO_2 + 14\ MnO + 62\ Mg^{2+} + 35\ H_2O$

MELTS predicts small quantities of quartz and biotite formation in the groundmass of these alkaline lavas. For the purpose of understanding gross weathering reactions, these small quantities have been neglected.

As reported by Nelson *et al.* (2013) and Sowards *et al.* (2018), these reactions indicate that much of the silica is released during weathering while the remainder is stored in the clays. Furthermore, silica concentration in solute flux is used as a proxy for weathering, as suggested in Sowards *et al. (*2017), Nelson *et al.* (2012), Goodfellow *et al.* (2015), and Brantley and White (2009), and shown by our τ calculations. In all of the Molokai samples, Si, Mn, Mg, Ca, Na, P and K have negative τ values which indicates leaching while Al and Fe have high positive τ values which indicates accumulation (Fig. 14; Tables 4 and 5). LWPs with higher precipitation tend to have increased τ values indicating the leaching of silica and other soluble minerals (Table 4).

CONCLUSIONS

The Hawaiian Islands provide an ideal environment to investigate tropical chemical weathering rates and processes due to the uniform single rock type of basalt, varying precipitation amounts, and age differences of the islands. Within this study, LWP depths are investigated as a function of rainfall gradients (<250–3500 mm/yr) over three islands with different ages of bedrock, including Oahu (~2 Ma), Molokai (~1 Ma) and Hawaii's Kohala Peninsula (~0.3 Ma).

The HVSR method was used to obtain laterite thickness measurements over broad areas on the Hawaiian Islands. Comparing annual precipitation to erosion-corrected laterite depths revealed varying LWP weathering trends for each island surveyed. These weathering trends are

supported by Tau, XRD, XRF, and weathering reactions data. These data show that basalt islands undergo chemical weathering, at a downward rate constrained by precipitation.

LWP data shows older basalt islands (>2 Ma) have a developed a mature laterite profile. With time (>4 Ma), the laterite profile thickens as water percolates deeper into the basalt. Intermediate-age basalt islands (~1 Ma) have a similar, albeit thinner, LWP. Although a laterite profile is present, it is still in a juvenile weathering phase. Sowards *et al.* (2018) suggest basalt weathers from the source of precipitation inward, with weathering occurring in different phases. Some parts of Molokai show signs of being in an intermediate weathering phase with several HVSR phase spectra that are featureless, most likely due to gradational weathering as seen by their step-like velocity-boundary velocity plots. HVSR data for younger basalt islands (<1 Ma), suggest that laterite thickness propagates upslope from the coast (Nelson *et al.,* 2020), eventually forming the same laterite profile seen on older islands.

REFERENCES

Asimow, P. D. and Ghiorso, M. S., 1998, Algorithmic modifications extending MELTS to calculate subsolidus phase relations: Mineral, v. 83, p. 1127–1132.

Beeson, M.H., 1976, Petrology, mineralogy, and geochemistry of the east Molokai volcanic series, Hawaii, USGS NO. 961, p. 1–53.

Brantley, S.L. and White, A.F., 2018, 10. Approaches to Modeling Weathered Regolith. Thermodynamics and Kinetics of Water-Rock Interaction, pp.435–484.

Castellaro S., Mulargia F., Bianconi L., 2005, Passive seismic stratigraphy: a new efficient, fast and economic technique, Geologia Tecnica e Ambientale 3: 76–102.

Chadwick, O.A., Gavenda, R.T., Kelly, E.F., Ziegler, K., Olson, C.G., Elliott, W.C. and Hendricks, D.M., 2003, The impact of climate on the biogeochemical functioning of volcanic soils, *Chemical Geology*, *202*(3–4), pp.195–223.

Clague, D.A., and Moore, J.G., 2002, The proximal part of the giant submarine Wailau landslide, Molokai, Hawaii: Journal of Volcanology and Geothermal Research, v. 113, nos. 1–2, p. 259–287.

Dailey, S.R., 2016, Geochemistry of the fluorine-and beryllium-rich Spor Mountain Rhyolite, Western Utah, Brigham Young University.

Dosseto, A., Turner, S.P., and Chappell, J., 2008, The evolution of weathering profiles through time: New insights from uranium-series isotopes, Earth and Planetary Science Letters, 274(3–4), pp.359–371.

Ferrier, K.L., Perron, J.T., Mukhopadhyay, S., Rosener, M., Stock, J.D., Huppert, K.L., Slosberg, M., 2013, Covariation of Climate and Long-term Erosion Rates Across a Steep Rainfall Gradient on the Hawaiian Island of Kaua'I. Geol. Soc. Am. Bull., 125 (7–8) (2013), pp. 1146–1163 doi:10.1130/B30726.1

Frazier, A. G., Giambelluca, T. W., Diaz, H. F. and Needham, H. L. (2016), Comparison of geostatistical approaches to spatially interpolate month-year rainfall for the Hawaiian Islands. Int. J. Climatol., 36(3), 1459–1470. doi: 10.1002/joc.4437

Gayer E., Michon L., Louvat P., Gaillardet J. 2019, Storm-induced precipitation variability control of long-term erosion. Earth and Planetary Science Letters 517: 61–70.

Ghiorso, M. S., and Sack, R. O., 1995, Chemical mass transfer in magmatic processes IV. A revised and internally consistent thermodynamic model for the interpolation and 21 extrapolation of liquid–solid equilibria in magmatic systems at elevated temperatures and pressures: Contributions to Mineralogy and Petrology, v. 119, p. 197–212.

Giambelluca, T.W., Q. Chen, A.G. Frazier, J.P. Price, Y.-L. Chen, P.-S. Chu, J.K. Eischeid, and D.M. Delparte, 2013: Online Rainfall Atlas of Hawai‘i. Bull. Amer. Meteor. Soc. 94, 313–316, doi: 10.1175/BAMS-D-11-00228.1.

Goodfellow, B.W., Chadwick, O.A., and Hiley, G.E., 2014. Depth and character of rock weathering across a basaltic-hosted climosequence on Hawai'i. *Earth Surface Processes and Landforms 39:381–398.*

Lau, L.S., and Mink, J.F., 2006, Hydrology of the Hawaiian Islands: University of Hawai'i Press, https://ebookcentral.proquest.com/lib/byu/reader.action?docID=3413305&ppg=40 (accessed March 2018).

Look, B.G., 2007, *Handbook of geotechnical investigation and design tables*. CRC Press:Leiden, Netherlands; 331.

Nelson, S.T., Barton, B., Burnett, M.W., McBride, J.H., Brown, L. and Spring, I., 2020, The lateral and vertical growth of laterite weathering profiles, Hawaiian Islands, USA. *Earth Surface Processes and Landforms*, *45*(12), pp.2940–2953. https://doi.org/10.1002/esp.4941

Nelson, S.T., Tingey, D.G., and Selck, B., 2013, The denudation of ocean islands by ground and surface waters: The effects of climate, soil thickness, and water contact times on Oahu, Hawaii: Geochimica et Cosmochimica Acta, v. 103, p. 276–294, doi:https://doi.org/10.1016/j.gca.2012.09.046

Nelson S., McBride J., 2019, Application of HVSR to estimating thickness of laterite weathering profiles in basalt. Earth Surf. Process. Landf. 2019, 44, 1365–1376. doi:https://doi.org/10.1002/esp.4580

Park C.B., Miller R.D., Xia J., Ivanov J., 2007, Multichannel analysis of surface waves (MASW)—active and passive methods. The Leading Edge ; 26 (1): 60–64. doi: https://doi.org/10.1190/1.2431832

Porder S., Hilley G.E., Chadwick O.A., 2007, Chemical weathering, mass loss, and dust inputs across a climate by time matrix in the Hawaiian Islands. Earth and planetary Science Letters 258:414–427.

Shade, P.J., 1995. Water budget for the Kohala area, Island of Hawaii (Vol. 95, No. 4114). US Department of the Interior, US Geological Survey.

Shade, P.J., 1997. Water budget for the island of Molokai, Hawaii (Vol. 97, No. 4155). US Geological Survey.

Shade P. J. and Nichols W. D. (1996) Water budget and the effects of land-use changes on ground-water recharge, Oahu, Hawaii. P. 1412-C, C1–C38.

Sherrod D.R., Sinton J.M., Watkins Sarah E., and Brunt Kelly M., 2007, Geologic map of the State of Hawai`i: U.S. Geological Survey Open-File Report 2007–1089 [http://pubs.usgs.gov/of/2007/1089/].

Sowards K., Nelson S.T., McBride J, Bickmore B., Tingey D., Rey K., Yaede JR. 2018. A conceptual model for the early weathering of ocean islands: a synthesis of geochemistry and geophysics, Kohala Peninsula, Hawaii, USA. Geosphere 14: 1–19.

Stearns, H.T., and Macdonald, G.A., 1946, Geology and ground-water resources of the island of Hawaii: Hawaii Division of Hydrography Bulletin 9, 363 p.

Stearns, H.T., and Macdonald, G.A., 1947, Geology and ground-water resources of the island of Molokai, Hawaii: Hawaii Division of Hydrography Bulletin 11, 113 p.

Stearns, H.T., and Vaksvik, K.N., 1935, Geology and ground- water resources of the island of Oahu, Hawaii: Hawaii Division of Hydrography Bulletin 1, 479 p.

Tolworthy, J.H., 2020. A Water Budget and Solute Flux Budget for Waimea River Watershed, Kauai, HI, USA (Doctoral dissertation, Brigham Young University).

U.S. Geological Survey, 2021, National Water Information System data available on the World Wide Web, https://maps.waterdata.usgs.gov/mapper/index.html (accessed September 2020).

U.S. Geological Survey, 2021, National Map Data Downloader available on the World Wide Web, https://apps.nationalmap.gov/downloader/#/ (accessed September 2020)

Wolfe, E.W., and Morris, Jean, 1996a, Geologic map of the Island of Hawaii: U.S. Geological Survey Miscellaneous Investigations Series I–2524-A, scale 1:100,000.

Wong, I.G., Stokoe, K.H., II, Cox, B.R., Yuan, J., Knudsen, K.L., Terra, F., Okubo, P., Lin, Y-C., 2011, Shear-wave velocity characterization of the USGS Hawaiian strong-motion network on the Island of Hawaii and development of an NEHRP Site-Class Map: Bulletin of the Seismological Society of America **101**: 2252– 2269.

Yaede, J.R., McBride, J.H., Nelson, S.T., Park, C.B., Flores, J.A., Turnbull, S.J., Tingey, D.G., Jacobsen, R.T., Dong, C.D., and Gardner, N.L., 2015, A geophysical strategy for measuring the thickness of the critical zone developed over basalt lavas: Geosphere, v. 11, p. 514–532, doi: 10.1130/GES01142.1.

FIGURES

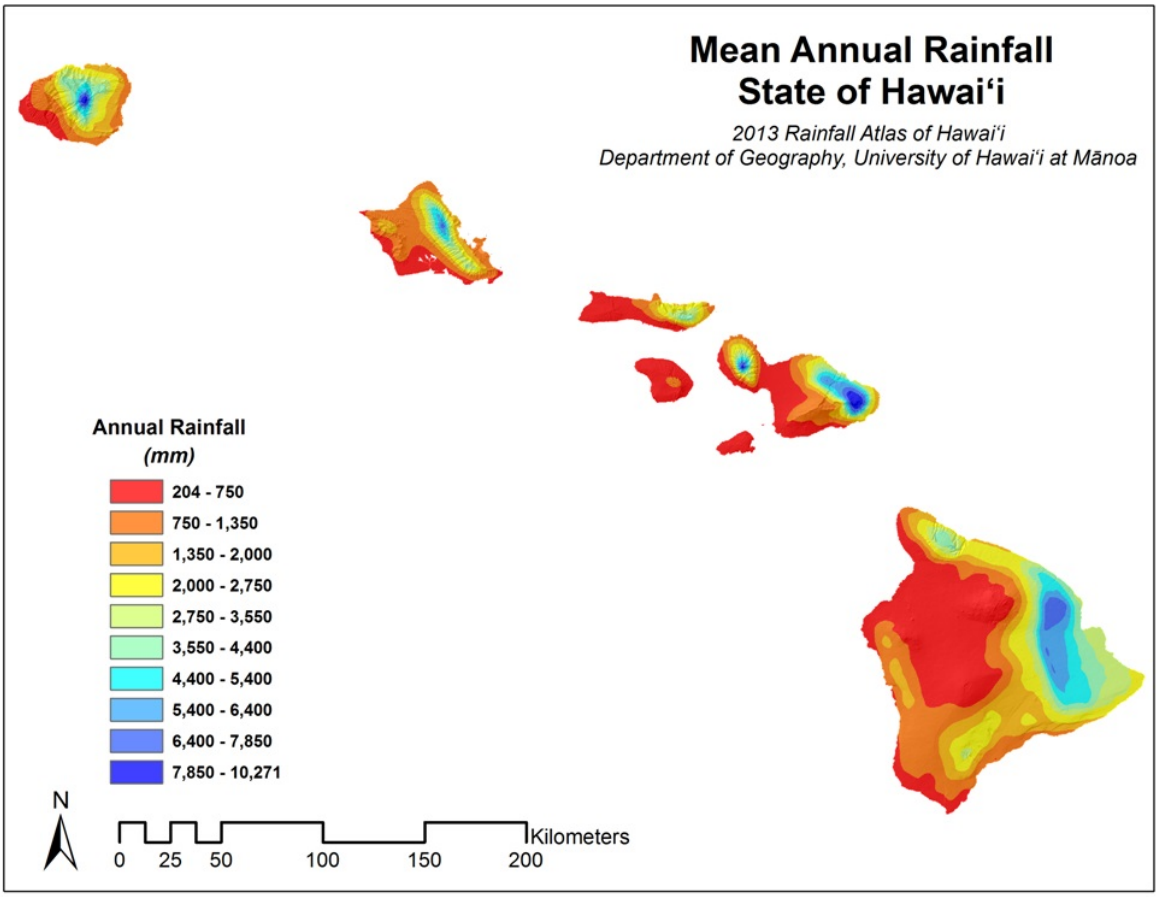

Figure 1. Annual rainfall (mm) for the state of Hawaii (Graphic from Giambelluca et al., 2013). The windward side of the island records more precipitation than the leeward side by an order of magnitude. This influences the rate of weathering as water is a primary factor for weathering reactions.

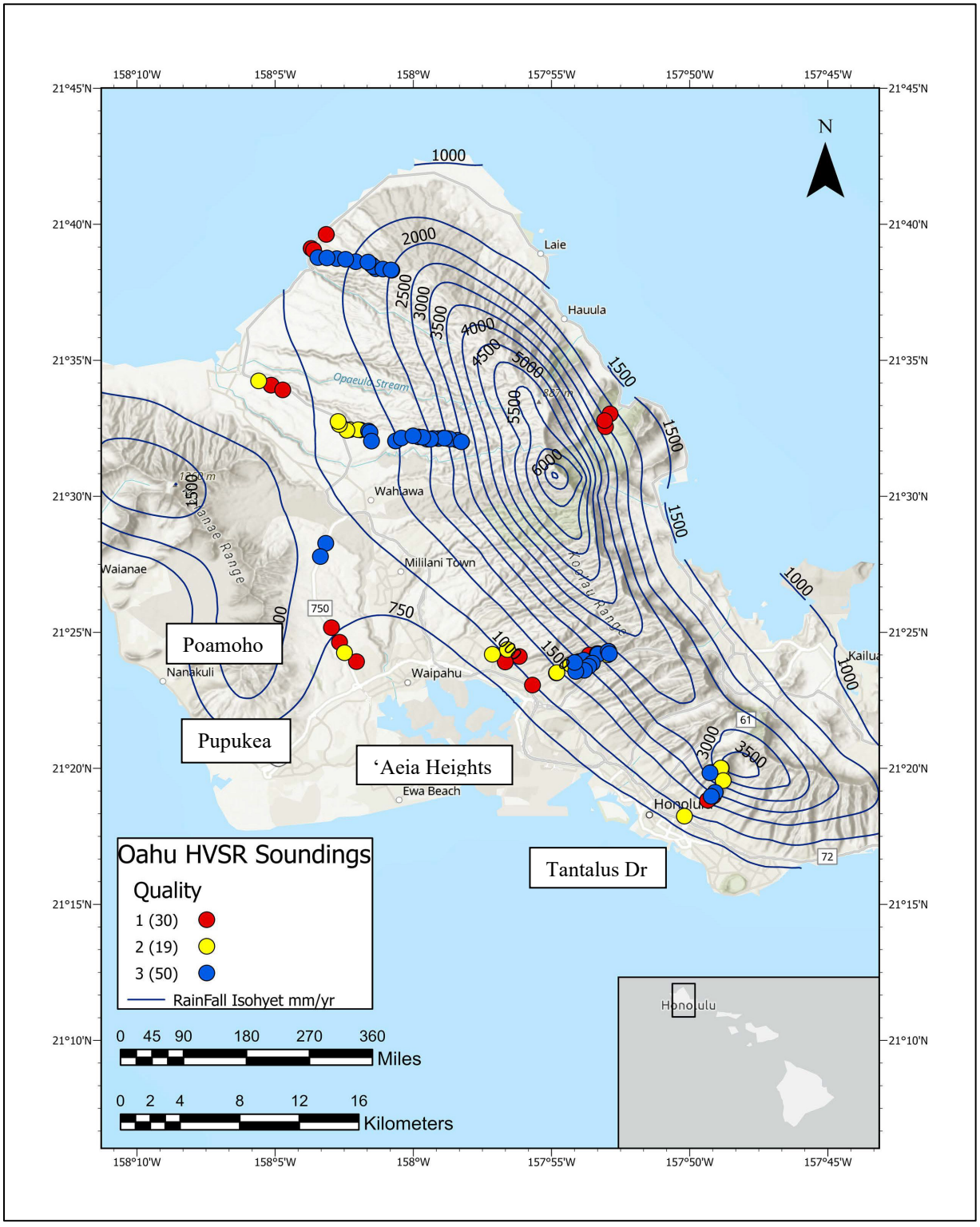

Figure 2. HVSR sounding locations on the island of Oahu. When possible, the sounding was taken on an interfluvial ridge. Land access and safety were also factored in when determining sounding locations. Refer to text for quality number explanation.

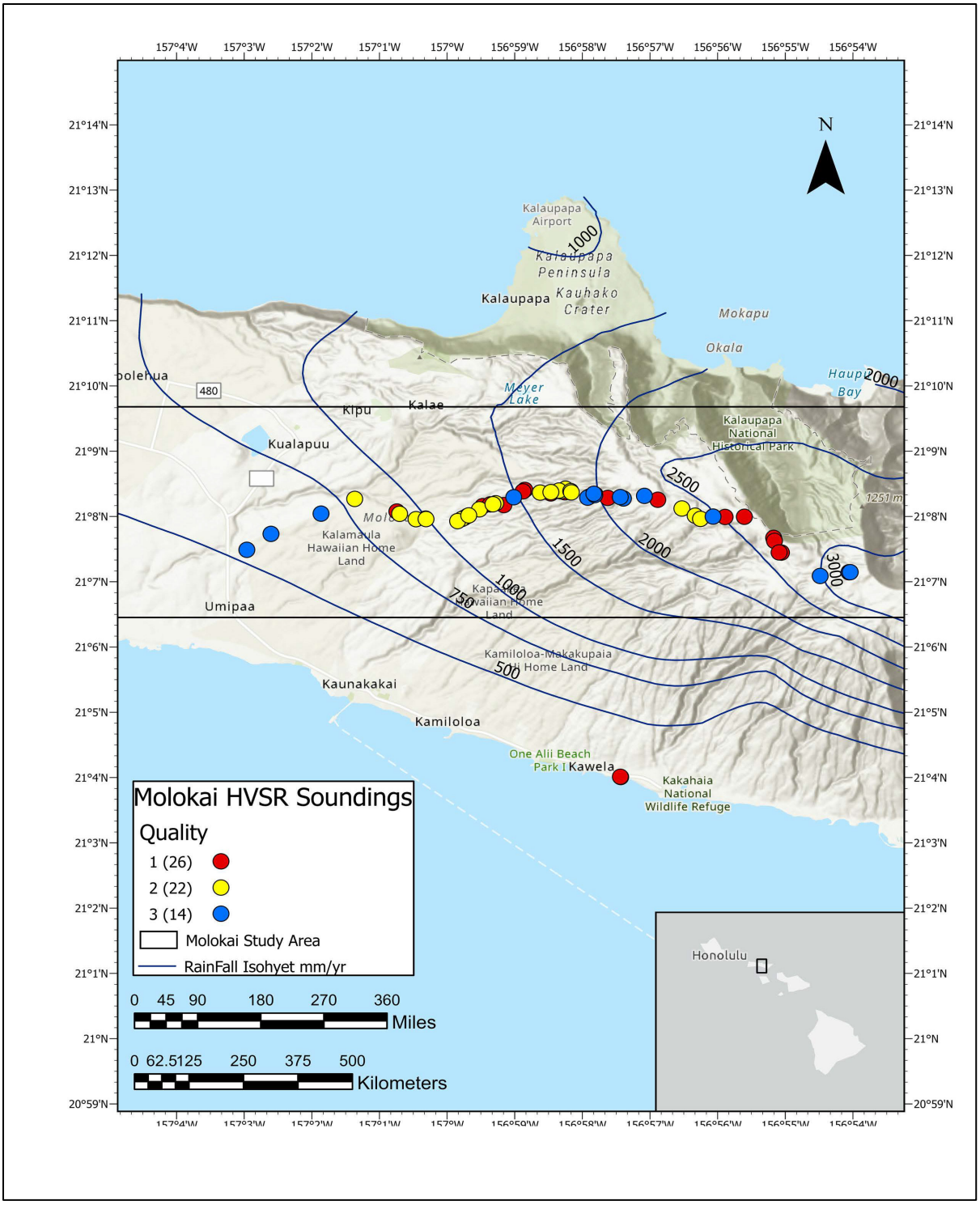

Figure 3. HVSR sounding locations on the island of Molokai. Soundings were taken across rainfall isohyets along a forest service road. Refer to the text for quality number explanation.

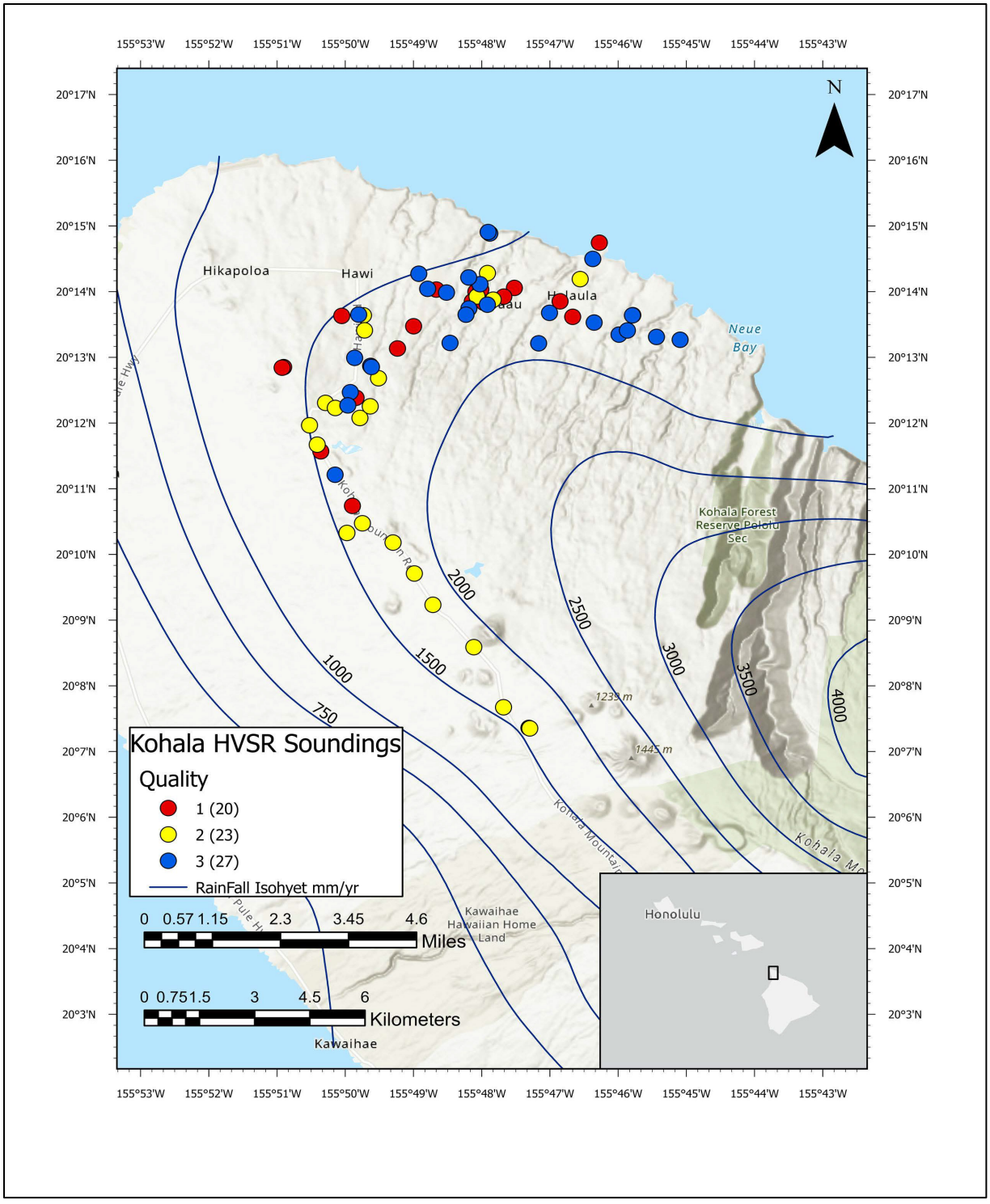

Figure 4. HVSR sounding locations on the island of Hawaii on the Kohala peninsula. Soundings were taken along route 250 and in public locations in and around Hawi, Hawaii. Refer to the text for quality number explanation.

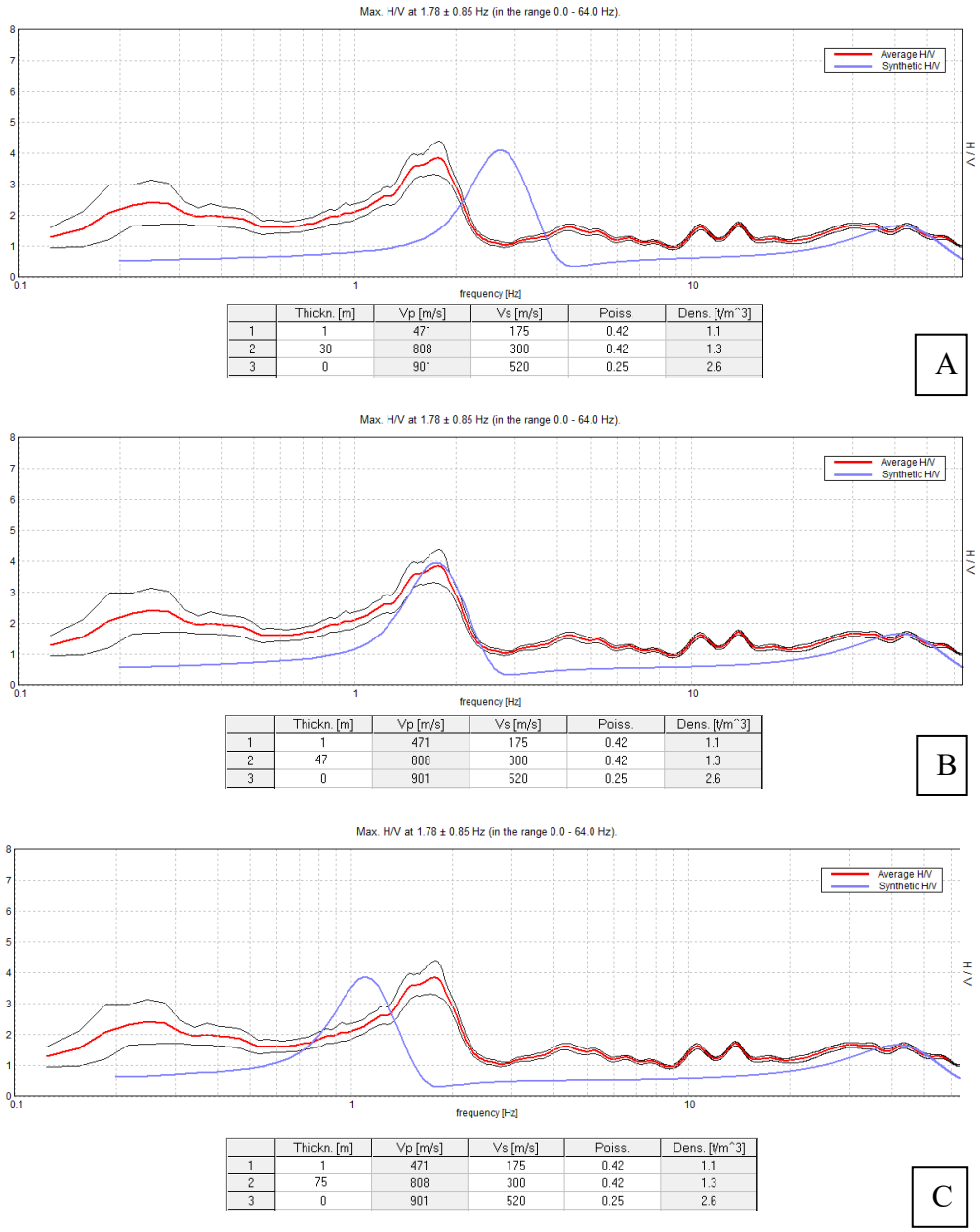

	Thickn. [m]	Vp [m/s]	Vs [m/s]	Poiss.	Dens. [t/m^3]
1	1	471	175	0.42	1.1
2	30	808	300	0.42	1.3
3	0	901	520	0.25	2.6

	Thickn. [m]	Vp [m/s]	Vs [m/s]	Poiss.	Dens. [t/m^3]
1	1	471	175	0.42	1.1
2	47	808	300	0.42	1.3
3	0	901	520	0.25	2.6

	Thickn. [m]	Vp [m/s]	Vs [m/s]	Poiss.	Dens. [t/m^3]
1	1	471	175	0.42	1.1
2	75	808	300	0.42	1.3
3	0	901	520	0.25	2.6

Figure 5. A single HVSR spectrum collected on Molokai with varying modeled laterite thickness plotted using Grilla (Castellaro et al., 2005). Several variables (Poisson's ratio, density, and laterite V_s (layer 2)) were held constant throughout the modeling process for all data samples. Altering laterite thickness changes the modeled peak along the x-axis. Image A uses a modeled thickness of 30 m, Image B uses a modeled thickness of 47 m, and Image C uses a modeled thickness of 75 m. Altering V_s of basalt will modify the amplitude peak of the model allowing a better fit.

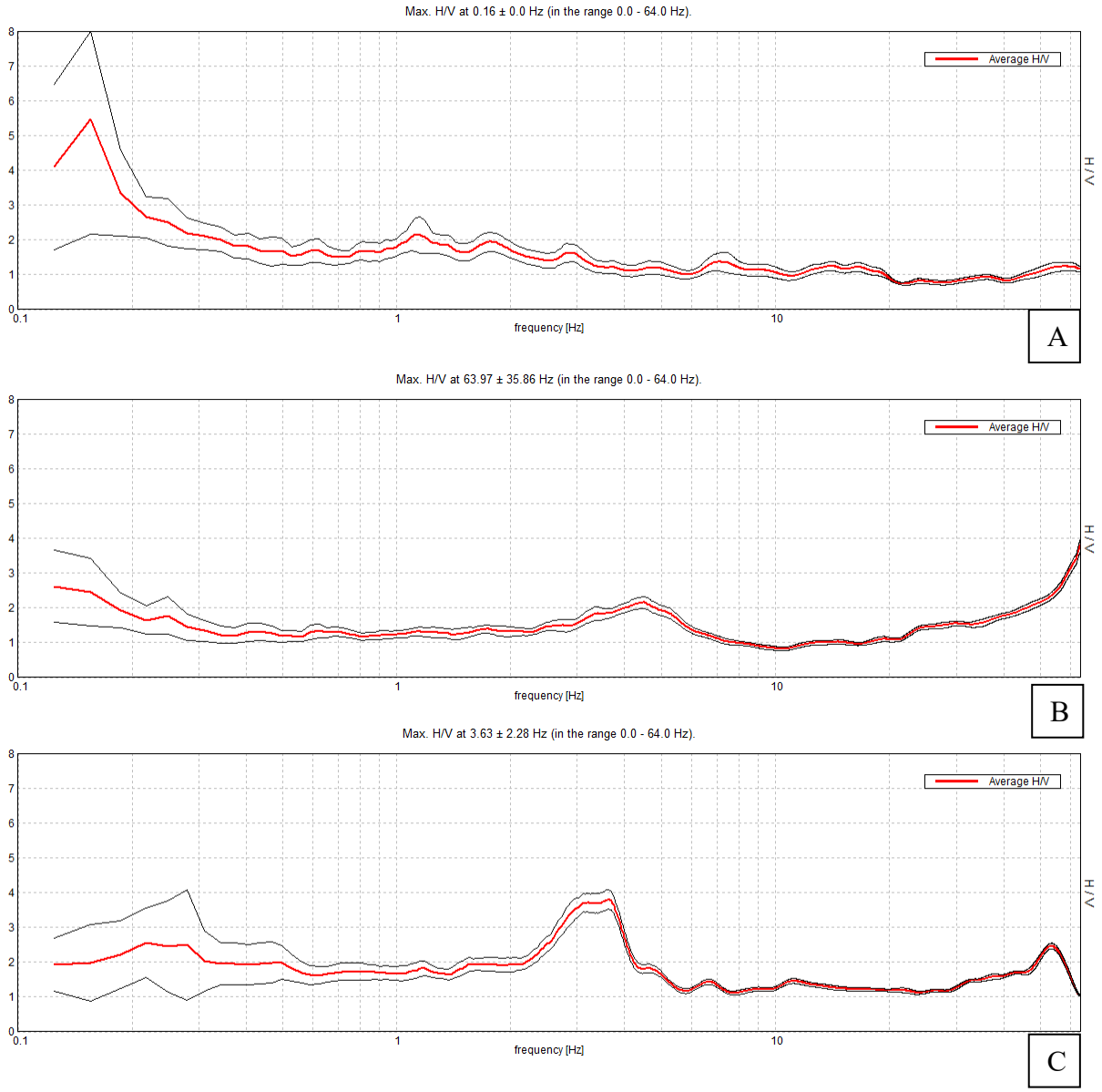

Figure 6. HVSR spectra plotted using the Grilla software (Castellaro et al., 2005). Images A, B, and C are spectra collected from Molokai that represent quality categories 1, 2, and 3, respectfully. As can be seen, category 1 spectrum are relatively featureless and flat, which resulted in no model. Category 2 spectrum have low-amplitude peaks with soft shoulders that are sometimes not distinct enough from the surrounding spectrum to be entirely unambiguous. Category 3 spectrum have clearly distinct peaks that stand out in the spectrum, allowing the model to have a good fit, with a high degree of confidence.

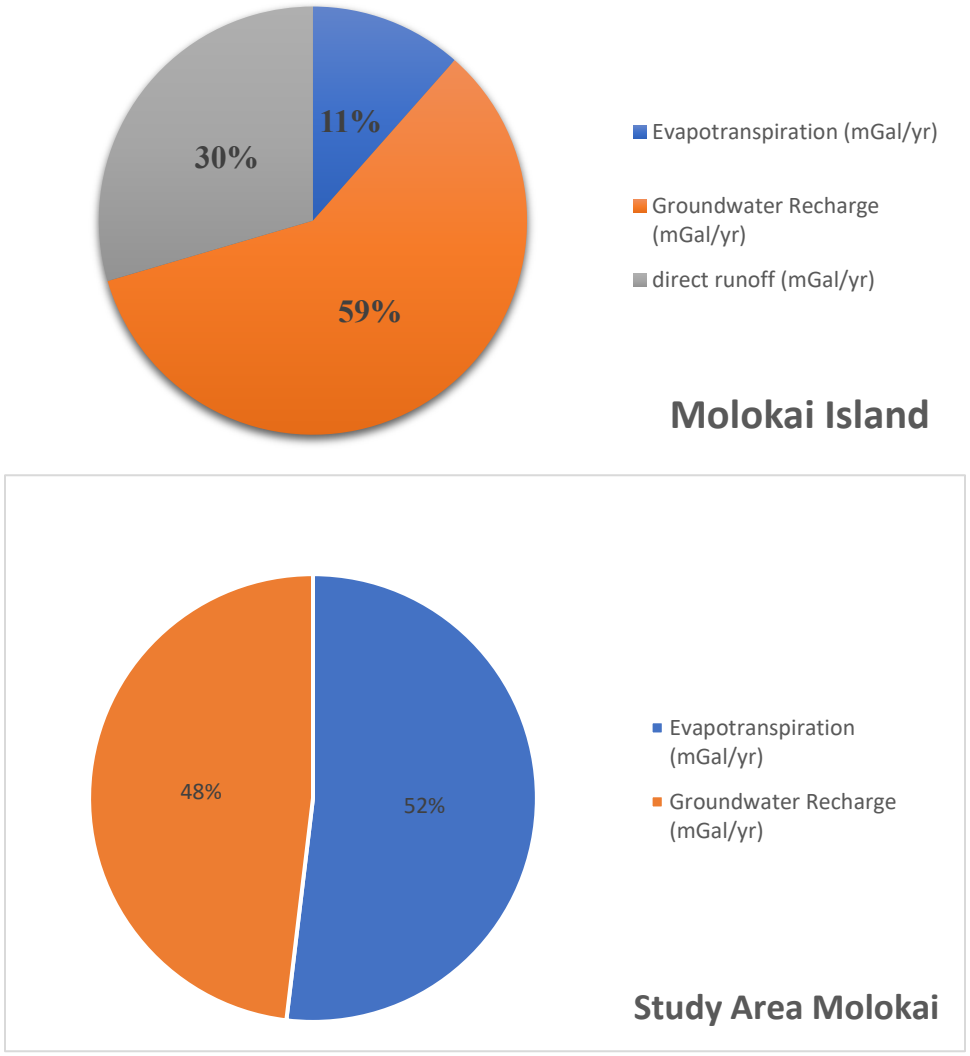

Figure 7. Water budgets for Molokai (Shade, 1997) and the study area in central Molokai (Giambelluca et al., 2013). The study area does not contain any perennial streams, thus there is no direct runoff component to its water budget.

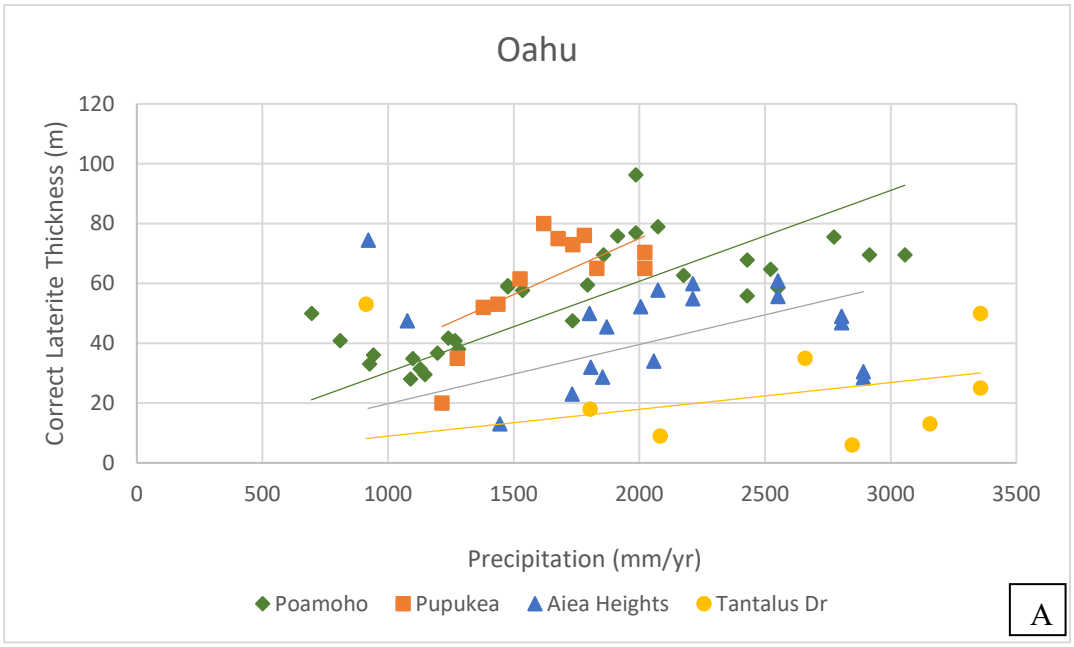

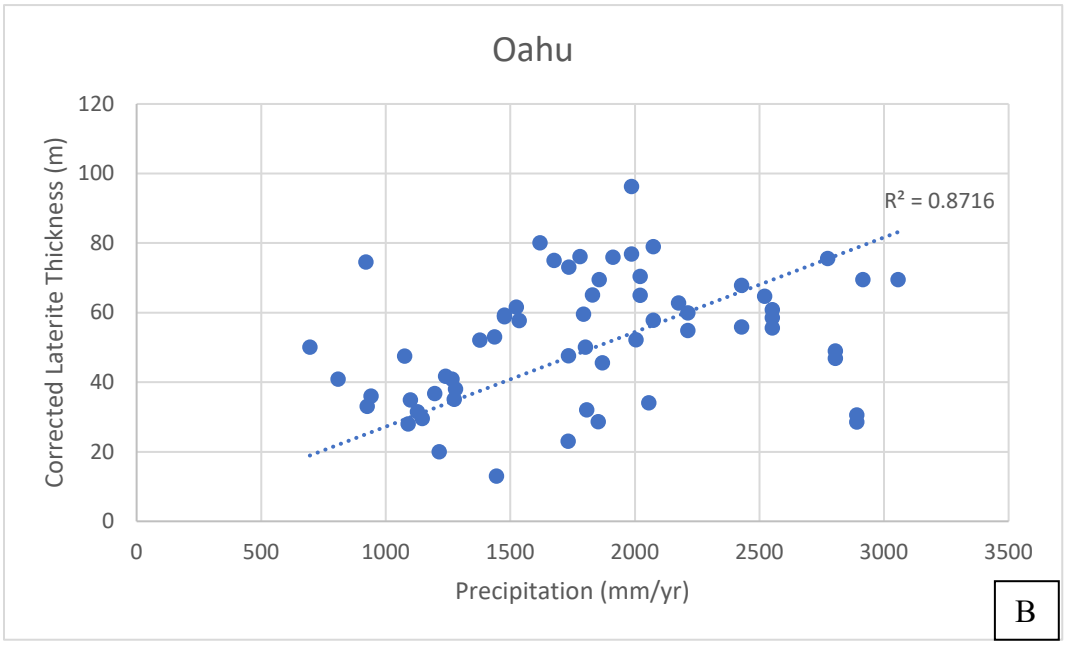

Figure 8. A) Oahu LWP thickness separated into four zones (Fig. 2). The three zones, Poamoho ($r^2 = 0.9396$), Pupukea ($r^2 = 0.965$), and Aiea Heights ($r^2 = 0.8273$), with soundings taken on older Ko'olau basalts show a positive trend between laterite thickness and precipitation compared to soundings taken on the younger Honolulu rejuvenation basalt (Tantalus Dr. $r^2 = 0.5794$) on the south side of Oahu. Due to the age difference between basalts, Tantalus Dr. soundings were not used for precipitation-LWP trends. B) Combining the zones, with the exception of Tantalus Dr., shows the overall trend for Oahu.

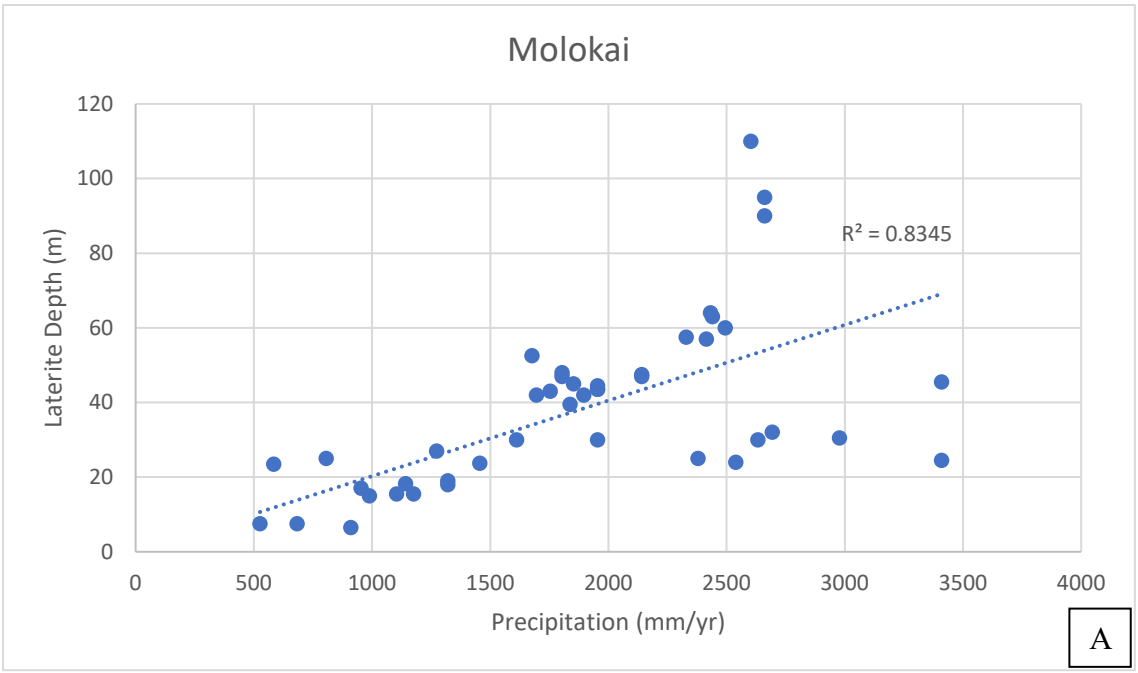

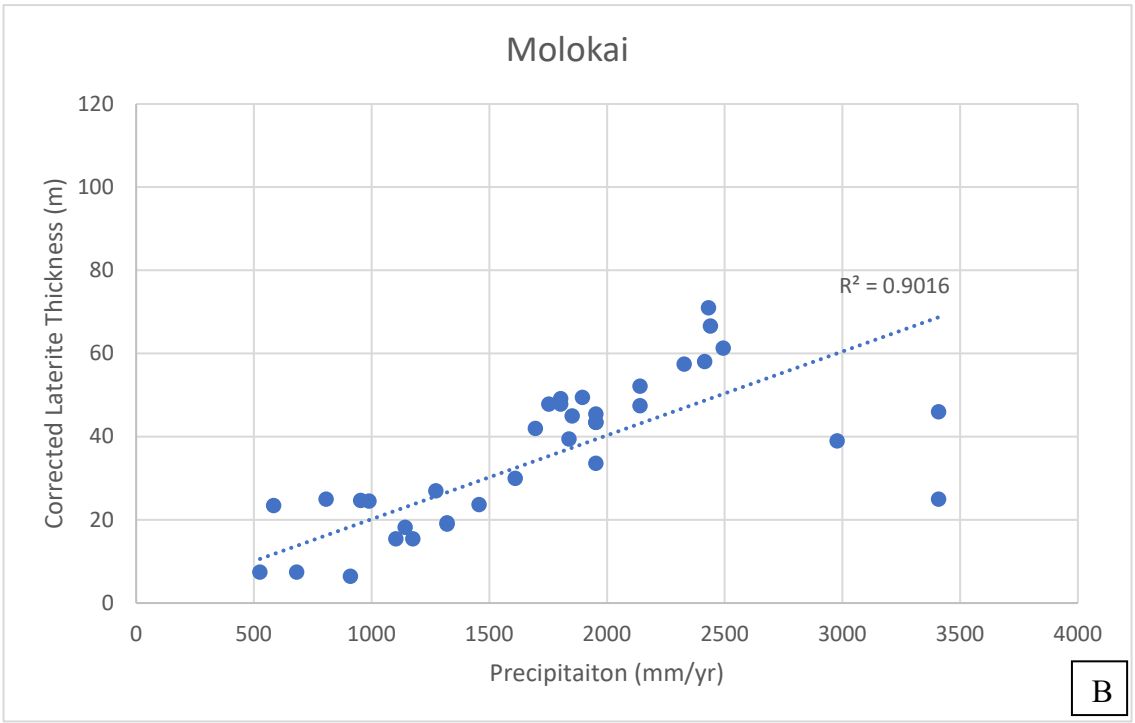

Figure 9. (A) Corrected laterite depth vs. precipitation including points extremely gradational LWPs. (B) Corrected laterite depth vs. precipitation excluding gradational spectra. When the gradational HVSR soundings are removed, r^2 value increases, suggesting there exists a relationship between LWP and precipitation values.

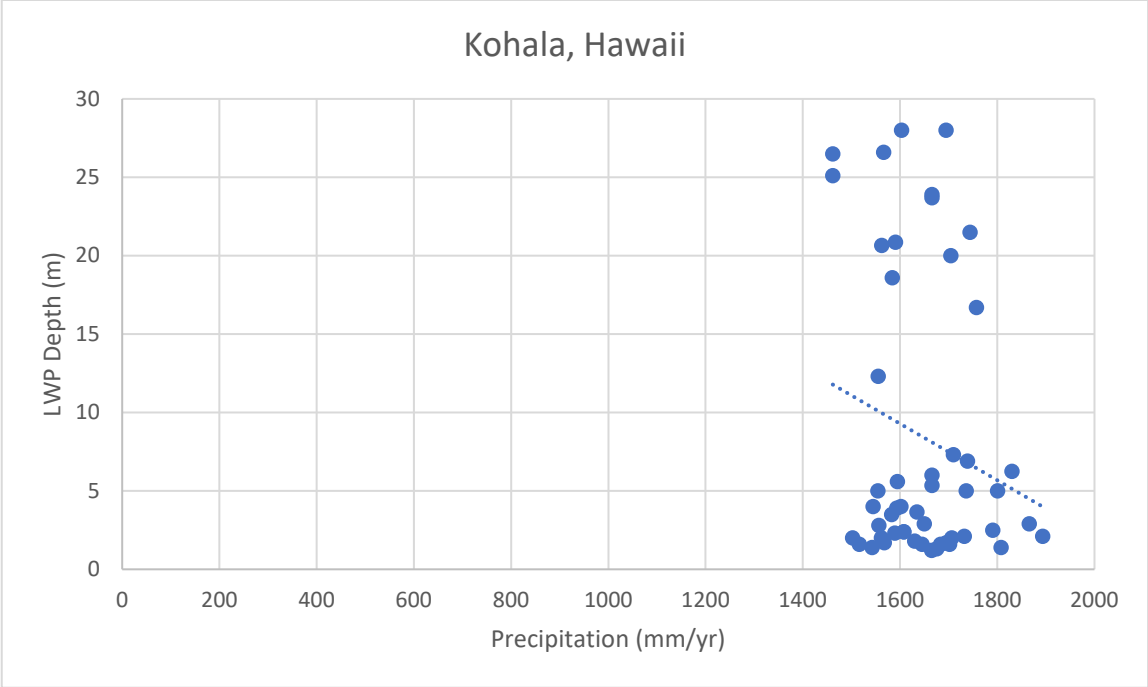

Figure 10. HVSR soundings collected within two contours of a precipitation gradient (1400–1900 mm/yr) in order to control precipitation as a factor. This revealed shallow LWPs at higher elevations and deeper LWPs closer to the coast. For a more detailed analysis on coastal laterite behavior, see Nelson et al. (2020).

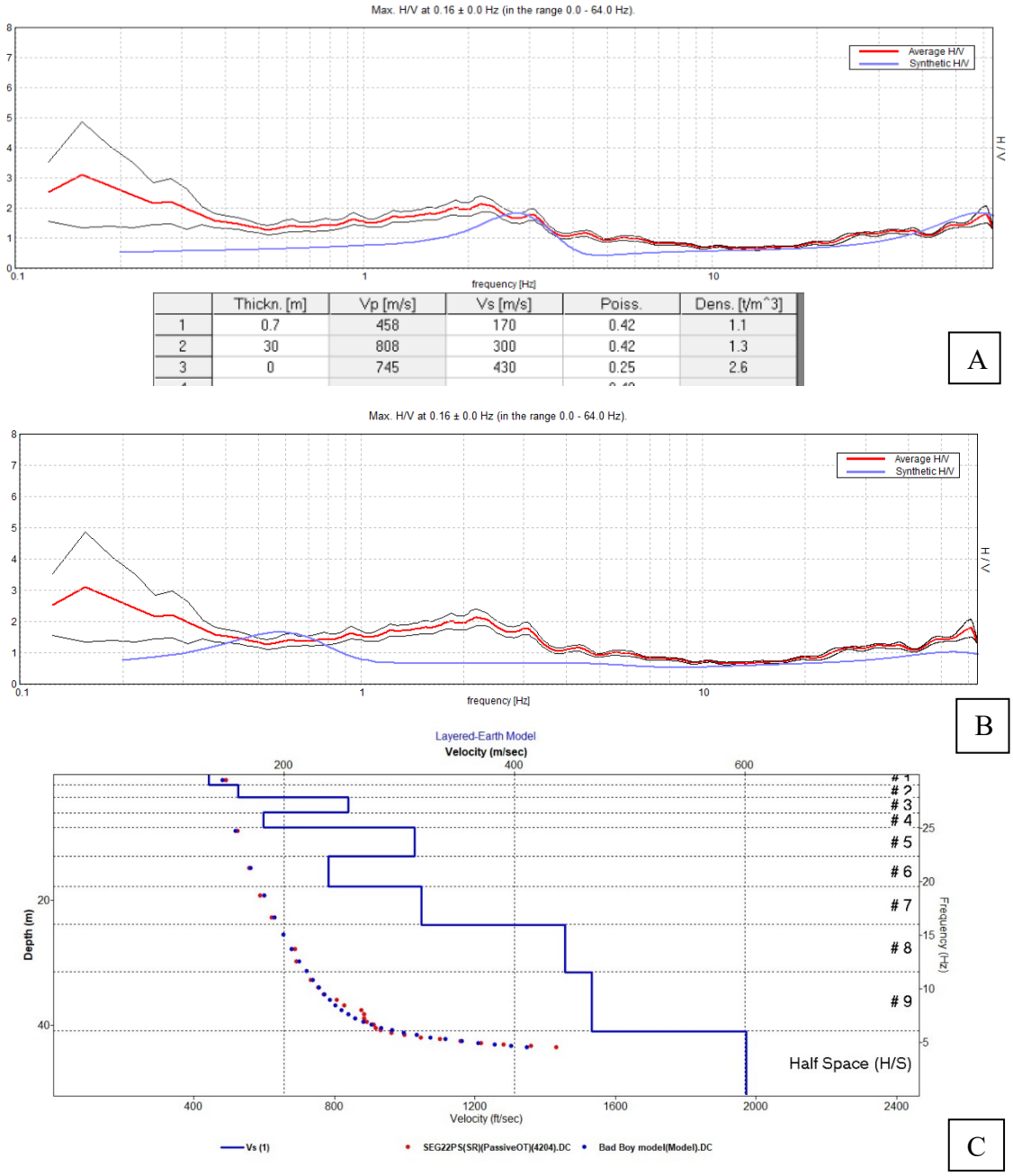

Figure 11. (A) HVSR spectra modeled in Grilla using the approach outlined in Nelson and McBride (2017). (B) Using the same HVSR spectra as in Image A, the data was fit with a 10-layer model with V_s and density increasing in each layer. (C) The MASW observed and modeled dispersion curve and model at the same location as the HVSR sounding. It is assumed that HVSR spectra exhibiting such a featureless pattern are LWPs undergoing gradational weathering and show no sharp V_s boundary as commonly seen on Oahu.

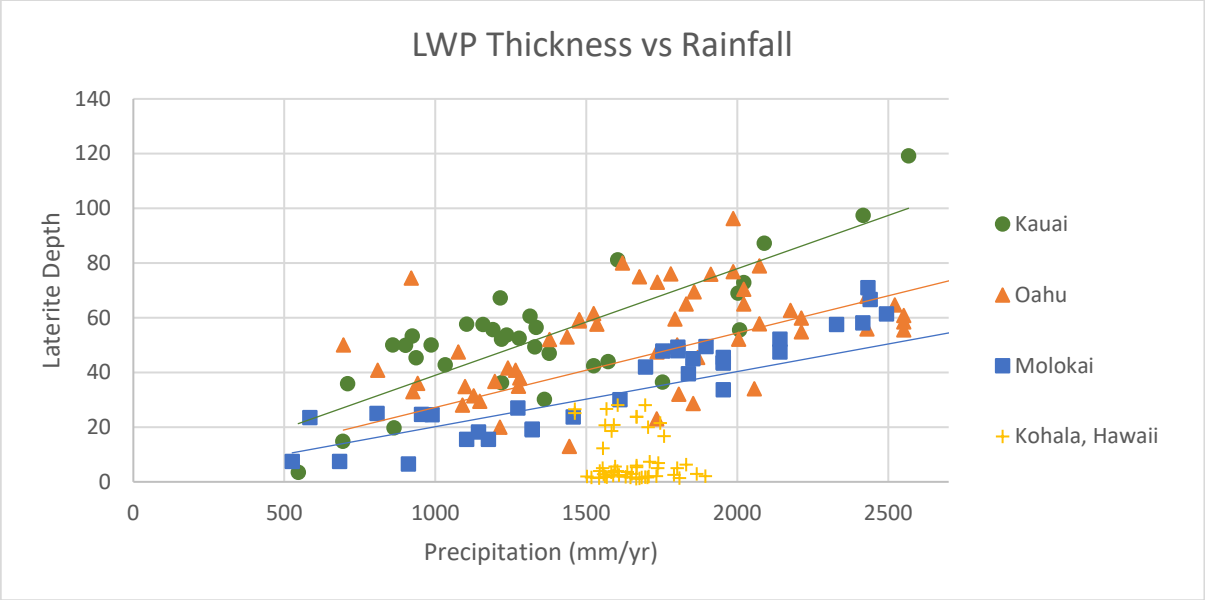

Figure 12. Laterite thickness plotted against annual rainfall across four islands. Trend lines show laterite depths increase with age for similar precipitations across Kauai (r^2=0.9406), Oahu (r^2=0.8716), and Molokai (r^2=0.9016). Kohala's soundings are constrained between the 1500 and 2000 mm/yr precipitation contours.

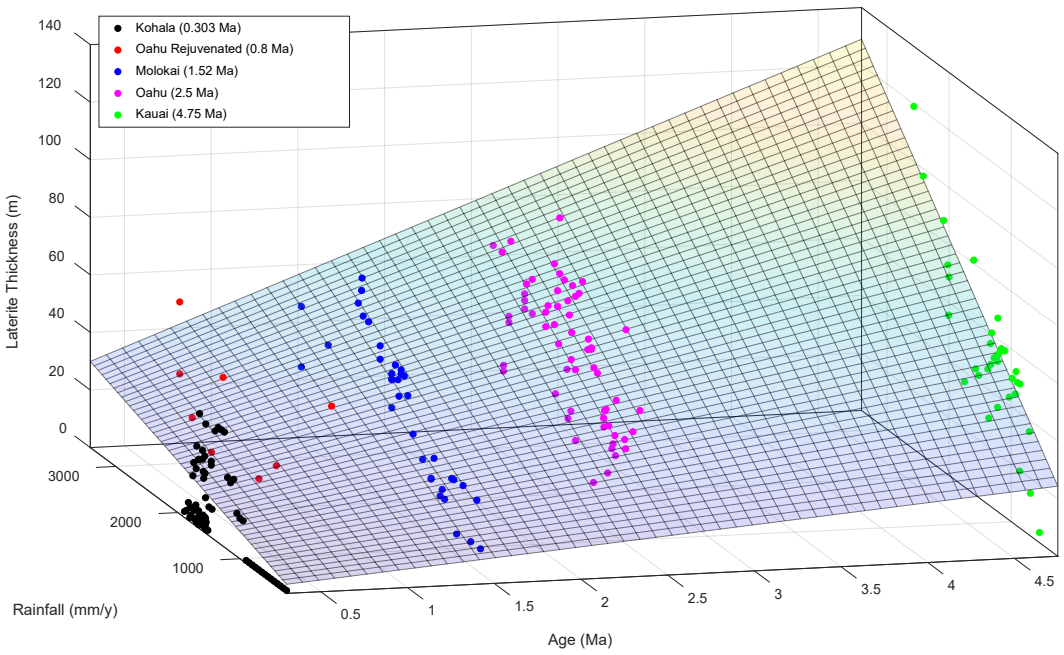

Figure 13. Laterite thickness data from Kauai, Oahu, Molokai, and Kohala are plotted on a 3-dimsional graph using Eq 4. (r^2=0.6182). By fixing one variable (age, precipitation, thickness), Eq 4 can be used to model potential laterite thickness trends from the other two variables. This model does not work at extremely low values of precipitation or age.

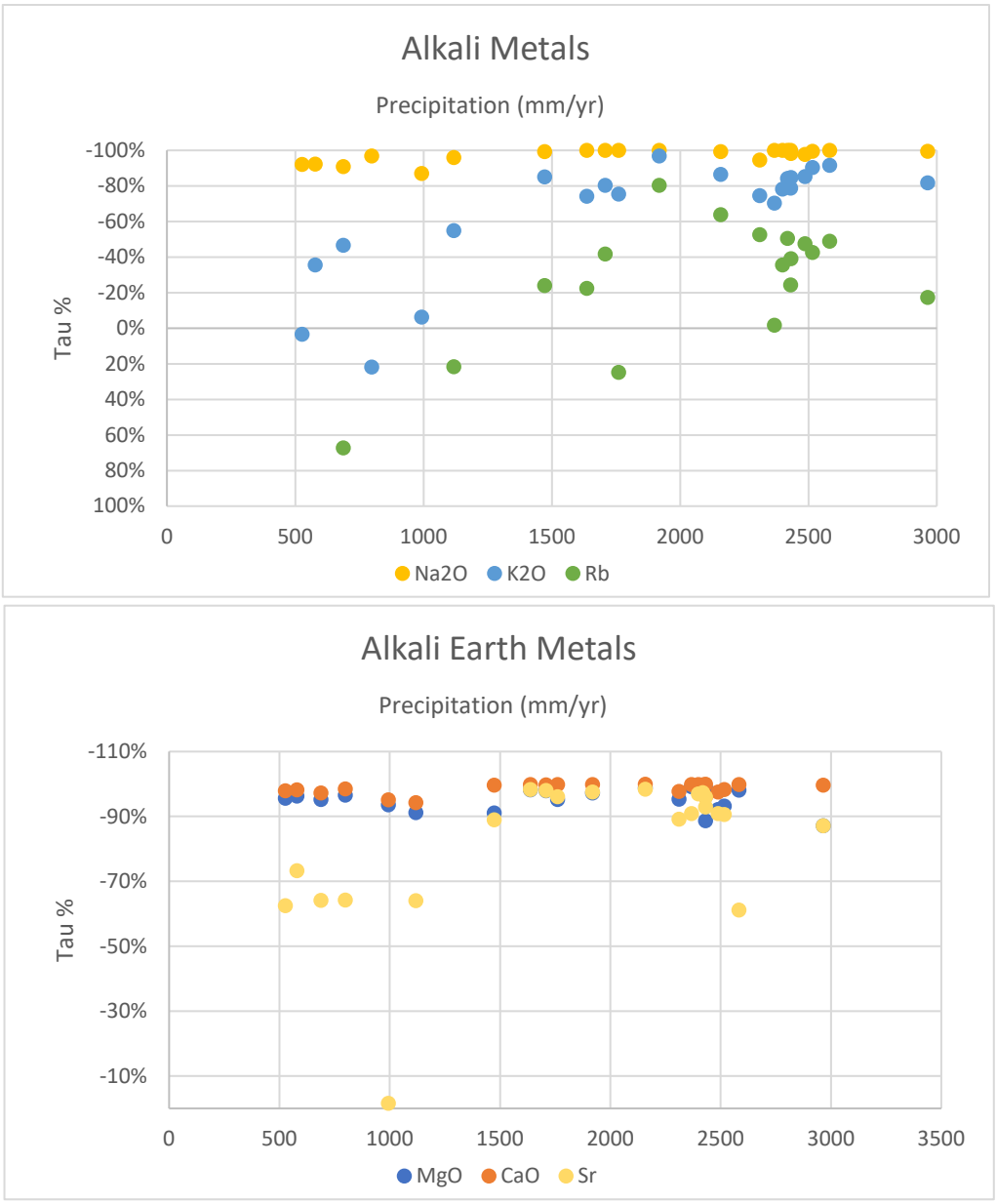

Figure 14. Na, K, Rb, Mg, Ca, and Sr values plotted as a function of precipitation. Parent basalt values from Beeson (1976) were used in Tau calculations. Increasing precipitation shows a general trend of decreasing Tau values, indicating these elements are being leached from the soil.

TABLES

Table 1. HVSR sounding information for Oahu

SITE	CORRECTED LATERITE THICKNESS (M)	RAINFALL (MM/Y)	QUALITY NUMBER	COMMENT	LONGITUDE	LATITUDE
O-DAY 1 07:30	38	1280	3	Koolau Basalt	158°01.6203 W	21°32.4010 N
O-DAY 1 07:47	41	1266	3	Koolau Basalt	158°01.5702 W	21°32.3546 N
O-DAY 1 08:38	42	1240	3	Koolau Basalt	158°01.5118 W	21°32.0296 N
O-DAY 1 09:28	59	1476	3	Koolau Basalt	158°00.6411 W	21°32.0335 N
O-DAY 1 09:28	59	1476	3	Koolau Basalt	158°00.6399 W	21°32.0355 N
O-DAY 1 10:27	77	1986	2	Koolau Basalt	157°59.4425 W	21°32.1008 N
O-DAY 1 10:41	76	1912	3	Koolau Basalt	157°59.4955 W	21°32.0988 N
O-DAY 1 11:13	63	2176	3	Koolau Basalt	157°59.0906 W	21°32.1218 N
O-DAY 1 11:25	56	2429	3	Koolau Basalt	157°58.9168 W	21°32.1439 N
O-DAY 1 12:00	65	2521	3	Koolau Basalt	157°58.6842 W	21°32.1056 N
O-DAY 1 12:14	76	2773	3	Koolau Basalt	157°58.4010 W	21°32.0639 N
O-DAY 1 12:37	70	2915	3	Koolau Basalt	157°58.2632 W	21°32.0058 N
O-DAY 1 12:48	70	3056	3	Koolau Basalt	157°58.2559 W	21°32.0030 N
O-DAY 1 13:29	59	2551	3	Koolau Basalt	157°58.7875 W	21°32.1310 N
O-DAY 1 13:30	68	2429	3	Koolau Basalt	157°58.8724 W	21°32.1353 N
O-DAY 1 14:07	79	2073	3	Koolau Basalt	157°59.2889 W	21°32.1290 N
O-DAY 1 14:13	96	1986	3	Koolau Basalt	157°59.3774 W	21°32.0982 N
O-DAY 1 14:54	70	1857	3	Koolau Basalt	157°59.6640 W	21°32.1713 N
O-DAY 1 14:56	60	1794	3	Koolau Basalt	157°59.8080 W	21°32.1862 N
O-DAY 1 15:30	48	1734	3	Koolau Basalt	158°00.0082 W	21°32.2235 N
O-DAY 1 15:43	58	1535	3	Koolau Basalt	158°00.4307 W	21°32.1432 N
O-DAY 2 15:38	37	1197	2	Koolau Basalt	158°01.9945 W	21°32.4502 N
O-DAY 2 16:37	30	1147	2	Koolau Basalt	158°02.3021 W	21°32.4499 N
O-DAY 2 16:40	32	1127	2	Koolau Basalt	158°02.4049 W	21°32.4276 N
O-DAY 5 08:01	41	809	2	Koolau Basalt	158°05.5972 W	21°34.2432 N
O-DAY 5 09:14	36	941	3	Koolau Basalt	158°03.1687 W	21°28.2740 N
O-DAY 5 09:18	33	926	3	Koolau Basalt	158°03.3604 W	21°27.7873 N
O-DAY 5 10:23	50	695	2	Koolau Basalt	158°02.4913 W	21°24.2505 N

O-DAY 5 15:07	35	1098	2	Koolau Basalt	158°02.6779 W	21°32.6412 N

Table 1 continued

SITE	CORRECTED LATERITE THICKNESS (M)	RAINFALL (MM/Y)	QUALITY NUMBER	COMMENT	LONGITUDE	LATITUDE
O-DAY 5 15:09	28	1089	2	Koolau Basalt	158°02.7229 W	21°32.7528 N
O-DAY 2 07:21	75	1676	3	Koolau Basalt	158°01.5124 W	21°38.5129 N
O-DAY 2 07:59	73	1735	3	Koolau Basalt	158°01.4386 W	21°38.4464 N
O-DAY 2 08:24	76	1780	3	Koolau Basalt	158°01.3552 W	21°38.3665 N
O-DAY 2 08:41	65	1830	3	Koolau Basalt	158°01.1001 W	21°38.3544 N
O-DAY 2 09:12	70	2021	3	Koolau Basalt	158°00.7811 W	21°38.3128 N
O-DAY 2 09:19	65	2021	3	Koolau Basalt	158°00.8086 W	21°38.3218 N
O-DAY 2 10:22	80	1619	3	Koolau Basalt	158°01.6400 W	21°38.6126 N
O-DAY 2 10:40	62	1525	3	Koolau Basalt	158°02.0875 W	21°38.6254 N
O-DAY 2 11:06	53	1436	3	Koolau Basalt	158°02.4490 W	21°38.7150 N
O-DAY 2 11:08	52	1378	3	Koolau Basalt	158°02.7704 W	21°38.7377 N
O-DAY 2 11:37	35	1275	3	Koolau Basalt	158°03.1248 W	21°38.7645 N
O-DAY 2 11:40	20	1214	3	Koolau Basalt	158°03.4495 W	21°38.7778 N
O-DAY 4 07:55	52	2004	3	Koolau Basalt	157°54.0057 W	21°23.9243 N
O-DAY 4 08:28	58	2073	3	Koolau Basalt	157°53.8364 W	21°23.9775 N
O-DAY 4 09:43	61	2551	3	Koolau Basalt	157°53.3387 W	21°24.2233 N
O-DAY 4 09:44	56	2551	3	Koolau Basalt	157°53.3217 W	21°24.1949 N
O-DAY 4 10:32	29	2891	3	Koolau Basalt	157°52.9376 W	21°24.3081 N
O-DAY 4 10:35	31	2891	3	Koolau Basalt	157°52.9460 W	21°24.3037 N
O-DAY 4 11:06	47	2804	3	Koolau Basalt	157°52.9086 W	21°24.2116 N
O-DAY 4 11:11	49	2804	2	Koolau Basalt	157°52.9649 W	21°24.1748 N
O-DAY 4 11:58	60	2212	3	Koolau Basalt	157°53.5265 W	21°23.8661 N
O-DAY 4 11:59	55	2212	3	Koolau Basalt	157°53.5266 W	21°23.8681 N
O-DAY 4 12:34	34	2056	3	Koolau Basalt	157°53.6534 W	21°23.7513 N
O-DAY 4 12:41	29	1853	3	Koolau Basalt	157°53.8125 W	21°23.6046 N
O-DAY 4 13:21	23	1733	3	Koolau Basalt	157°54.1235 W	21°23.5609 N
O-DAY 4 13:36	50	1801	2	Koolau Basalt	157°54.1023 W	21°23.7281 N
O-DAY 4 14:28	32	1806	2	Koolau Basalt	157°54.3033 W	21°23.8165 N

Table 1 continued

SITE	CORRECTED LATERITE THICKNESS (M)	RAINFALL (MM/Y)	QUALITY NUMBER	COMMENT	LONGITUDE	LATITUDE
O-DAY 4 14:31	46	1869	3	Koolau Basalt	157°54.1639 W	21°23.8912 N
O-DAY 4 15:13	13	1444	2	Koolau Basalt	157°54.8061 W	21°23.5203 N
O-DAY 5 13:17	47	1076	2	Koolau Basalt	157°56.5937 W	21°24.3689 N
O-DAY 5 13:58	74	920	2	Koolau Basalt	157°57.1420 W	21°24.1912 N
O-DAY 3 08:55	53	913	2	Alluvium/Honolulu Volcanics	157°50.1925 W	21°18.2420 N
O-DAY 3 09:48	13	3156	2	Honolulu Volcanics	157°48.8730 W	21°19.8437 N
O-DAY 3 10:53	25	3357	2	Honolulu Volcanics	157°48.8723 W	21°20.0142 N
O-DAY 3 10:54	50	3357	2	Honolulu Volcanics	157°48.8586 W	21°20.0119 N
O-DAY 3 12:03	35	2659	3	Honolulu Volcanics	157°49.2650 W	21°19.8349 N
O-DAY 3 12:54	6	2847	2	Honolulu Volcanics	157°48.7876 W	21°19.5505 N
O-DAY 3 13:48	9	2083	3	Honolulu Volcanics	157°49.0793 W	21°19.1182 N
O-DAY 3 15:05	18	1803	2	Honolulu Volcanics	157°49.2202 W	21°18.9721 N
O-DAY 2 12:30			1	No Model	158°03.6951 W	21°39.1147 N
O-DAY 2 12:31			1	No Model	158°03.6083 W	21°39.0520 N
O-DAY 2 13:15			1	No Model	158°03.1522 W	21°39.6318 N
O-DAY 2 13:15			1	No Model	158°03.1471 W	21°39.6259 N
O-DAY 2 15:25			1	out of area	157°52.8779 W	21°33.0309 N
O-DAY 2 15:37			1	out of area	157°53.0499 W	21°32.5559 N
O-DAY 2 15:55			1	out of area	157°53.0805 W	21°32.7830 N
O-DAY 2 16:10			1	No Model	158°01.9236 W	21°32.4422 N
O-DAY 3 08:55			1	No Model	157°50.1255 W	21°18.2149 N
O-DAY 3 09:51			1	No Model	157°48.8696 W	21°19.8633 N
O-DAY 3 11:55			1	No Model	157°49.2295 W	21°19.8507 N
O-DAY 3 12:53			1	No Model	157°48.7892 W	21°19.5524 N
O-DAY 3 13:44			1	No Model	157°49.0767 W	21°19.1163 N
O-DAY 3 14:20			1	No Model	157°49.3527 W	21°18.8303 N
O-DAY 3 14:21			1	No Model	157°49.2817 W	21°18.8844 N
O-DAY 3 15:07			1	No Model	157°49.1463 W	21°18.9836 N
O-DAY 4 07:58			1	No Model	157°54.0005 W	21°23.9298 N
O-DAY 4 08:28			1	No Model	157°53.8338 W	21°23.9679 N
O-DAY 4 09:05			1	No Model	157°53.6401 W	21°24.1549 N
O-DAY 4 09:08			1	No Model	157°53.6340 W	21°24.1659 N
O-DAY 4 15:12			1	No Model	157°54.8203 W	21°23.5068 N
O-DAY 5 08:04			1	No Model	158°05.1453 W	21°34.0854 N
O-DAY 5 08:25			1	No Model	158°05.1451 W	21°34.0886 N
O-DAY 5 08:29			1	No Model	158°04.7263 W	21°33.9131 N
O-DAY 5 09:56			1	No Model	158°02.9614 W	21°25.1742 N
O-DAY 5 09:59			1	No Model	158°02.6700 W	21°24.6345 N
O-DAY 5 10:34			1	No Model	158°02.0561 W	21°23.9221 N
O-DAY 5 12:31			1	No Model	157°55.6876 W	21°23.0622 N
O-DAY 5 13:21			1	No Model	157°56.6746 W	21°23.9098 N
O-DAY 5 13:48			1	No Model	157°56.1658 W	21°24.1139 N

Table 2. HVSR sounding information for Molokai

SITE	CORRECTED LATERITE THICKNESS (M)	RAINFALL (MM/YR)	QUALITY NUMBER	COMMENT	LONGITUDE	LATITUDE
M-DAY 1 13:32	61	2494	3	East Molokai Volcanics	156°56.0673 W	21°07.9983 N
M-DAY 1 13:38	67	2439	2	East Molokai Volcanics	156°56.5279 W	21°08.1230 N
M-DAY 1 14:00	58	2415	2	East Molokai Volcanics	156°56.2528 W	21°07.9629 N
M-DAY 1 14:11	71	2432	2	East Molokai Volcanics	156°56.3317 W	21°08.0118 N
M-DAY 1 14:52	52	2141	3	East Molokai Volcanics	156°57.3932 W	21°08.2759 N
M-DAY 1 15:51	58	2328	3	East Molokai Volcanics	156°57.0824 W	21°08.3156 N
M-DAY 2 11:18	46	3409	3	East Molokai Volcanics	156°54.0392 W	21°07.1463 N
M-DAY 2 11:24	25	3409	3	East Molokai Volcanics	156°54.0578 W	21°07.1457 N
M-DAY 2 12:14	39	2978	3	East Molokai Volcanics	156°54.4874 W	21°07.0886 N
M-DAY 2 14:12	34	1954	2	East Molokai Volcanics	156°57.8925 W	21°08.3062 N
M-DAY 2 14:20	48	1753	2	East Molokai Volcanics	156°58.3459 W	21°08.3972 N
M-DAY 2 14:55	30	1611	2	East Molokai Volcanics	156°58.6237 W	21°08.3665 N
M-DAY 2 15:00	24	1456	3	East Molokai Volcanics	156°59.0158 W	21°08.2942 N
M-DAY 2 15:42	16	1103	2	East Molokai Volcanics	156°59.8450 W	21°07.9292 N
M-DAY 2 15:47	25	989	2	East Molokai Volcanics	157°00.3128 W	21°07.9605 N
M-DAY 2 16:21	25	807	2	East Molokai Volcanics	157°01.3682 W	21°08.2690 N
M-DAY 2 16:29	8	682	3	East Molokai Volcanics	157°01.8639 W	21°08.0436 N
M-DAY 2 17:00	24	584	3	East Molokai Volcanics	157°02.6056 W	21°07.7325 N
M-DAY 2 17:01	8	526	3	East Molokai Volcanics	157°02.9604 W	21°07.4896 N
M-DAY 3 09:27	7	910	2	East Molokai Volcanics	157°00.7037 W	21°08.0406 N
M-DAY 3 09:57	25	954	2	East Molokai Volcanics	157°00.4597 W	21°07.9594 N
M-DAY 3 10:45	18	1142	2	East Molokai Volcanics	156°59.7820 W	21°07.9617 N
M-DAY 3 11:24	27	1273	2	East Molokai Volcanics	156°59.5218 W	21°08.1094 N
M-DAY 3 12:06	19	1321	2	East Molokai Volcanics	156°59.2817 W	21°08.2030 N
M-DAY 3 13:29	49	1803	2	East Molokai Volcanics	156°58.3178 W	21°08.3857 N
M-DAY 3 14:11	48	1803	2	East Molokai Volcanics	156°58.2503 W	21°08.4256 N
M-DAY 3 14:51	46	1954	2	East Molokai Volcanics	156°57.8332 W	21°08.3365 N
M-DAY 3 15:34	48	2141	3	East Molokai Volcanics	156°57.4391 W	21°08.2976 N
M-DAY 3 16:15	49	1896	3	East Molokai Volcanics	156°57.9224 W	21°08.2884 N
M-DAY 4 10:15	16	1176	2	East Molokai Volcanics	156°59.6800 W	21°08.0173 N
M-DAY 4 10:52	19	1321	2	East Molokai Volcanics	156°59.3220 W	21°08.1866 N
M-DAY 4 14:31	44	1954	3	East Molokai Volcanics	156°57.8292 W	21°08.3478 N
M-DAY 4 14:33	44	1954	3	East Molokai Volcanics	156°57.8131 W	21°08.3286 N
M-DAY 4 15:13	40	1838	2	East Molokai Volcanics	156°58.1677 W	21°08.3688 N
M-DAY 4 15:17	45	1853	2	East Molokai Volcanics	156°58.1736 W	21°08.3894 N
M-DAY 4 15:50	42	1696	2	East Molokai Volcanics	156°58.4663 W	21°08.3738 N

Table 2 Continued

SITE	CORRECTED LATERITE THICKNESS (M)	RAINFALL (MM/YR)	QUALITY NUMBER	COMMENT	LONGITUDE	LATITUDE
M-DAY 1 10:34			1	No Model	156°55.6046 W	21°07.9954 N
M-DAY 1 10:35			1	No Model	156°55.8899 W	21°07.9933 N
M-DAY 1 14:43			1	No Model	156°56.7794 W	21°08.2515 N
M-DAY 1 15:13			1	No Model	156°57.0822 W	21°08.3072 N
M-DAY 1 15:22			1	No Model	156°56.8850 W	21°08.2568 N
M-DAY 3 09:22			1	No Model	157°00.7432 W	21°08.0756 N
M-DAY 3 10:03			1	No Model	157°00.3192 W	21°07.9650 N
M-DAY 3 10:49			1	No Model	156°59.6970 W	21°08.0085 N
M-DAY 3 11:28			1	No Model	156°59.4724 W	21°08.1586 N
M-DAY 3 12:17			1	No Model	156°59.1610 W	21°08.1745 N
M-DAY 3 12:51			1	No Model	156°58.8500 W	21°08.4079 N
M-DAY 3 12:55			1	No Model	156°58.8780 W	21°08.3847 N
M-DAY 3 13:32			1	No Model	156°58.4486 W	21°08.3677 N
M-DAY 3 14:07			1	No Model	156°58.2589 W	21°08.3711 N
M-DAY 3 14:51			1	No Model	156°57.8093 W	21°08.3341 N
M-DAY 3 15:40			1	No Model	156°57.6236 W	21°08.2852 N
M-DAY 3 16:25			1	No Model	156°58.1677 W	21°08.3688 N
M-DAY 4 05:57				Out of Area	156°57.4335 W	21°04.0086 N
M-DAY 4 05:58				Out of Area	156°57.4385 W	21°04.0121 N
M-DAY 4 09:29			1	No Model	157°00.3166 W	21°07.9680 N
M-DAY 4 09:31			1	No Model	157°00.3164 W	21°07.9635 N
M-DAY 4 10:10			1	No Model	156°59.7487 W	21°07.9779 N
M-DAY 4 10:58			1	No Model	156°59.3613 W	21°08.1860 N
M-DAY 4 12:48			1	No Model	156°55.1720 W	21°07.6730 N
M-DAY 4 12:50			1	No Model	156°55.1590 W	21°07.6256 N
M-DAY 4 13:22			1	No Model	156°55.0568 W	21°07.4470 N
M-DAY 4 13:26			1	No Model	156°55.0911 W	21°07.4503 N
M-DAY 4 15:53			1	No Model	156°58.4681 W	21°08.3537 N

Table 3. HVSR sounding information for Kohala.

SITE	CORRECTED LATERITE THICKNESS (M)	RAINFALL (MM/Y)	QUALITY NUMBER	COMMENT	LONGITUDE	LATITUDE
BI-DAY 1 09:03	7	1709.7	3	Pololu substrate	-155.7986056	20.22467833
BI-DAY 1 12:24	24	1666.1	2	Pololu substrate	-155.7630859	20.22735
BI-DAY 1 12:26	24	1666.1	3	Pololu substrate	-155.7631725	20.22731234
BI-DAY 1 13:07	7	1717.6	3	Pololu substrate	-155.7725209	20.22548414
BI-DAY 1 14:39	2	1695.2	3	Pololu substrate	-155.8053495	20.22440567
BI-DAY 1 15:29	2	1702.0	2	Pololu substrate	-155.8252033	20.21136999
BI-DAY 1 16:08	2	1683.5	2	Pololu substrate	-155.8297467	20.20128667
BI-DAY 1 16:11	2	1706.9	2	Pololu substrate	-155.8272383	20.20424166
BI-DAY 2 09:54	3	1556.8	2	Pololu substrate	-155.8381581	20.20512287
BI-DAY 2 10:02	2	1516.4	2	Pololu substrate	-155.8420685	20.19942202
BI-DAY 2 10:45	2	1567.7	2	Pololu substrate	-155.8329095	20.17210655
BI-DAY 2 13:36	5	1554.4	3	Pololu substrate	-155.8358172	20.18686659
BI-DAY 2 13:57	1	1542.6	2	Pololu substrate	-155.8401933	20.19452
BI-DAY 2 14:49	4	1635.1	2	Pololu substrate	-155.82913	20.17456
BI-DAY 2 14:52	3	1790.6	2	Pololu substrate	-155.8224345	20.16547526
BI-DAY 2 15:27	6	1830.7	2	Pololu substrate	-155.8164517	20.16183
BI-DAY 2 15:30	1	1807.8	2	Hawi substrate	-155.81191	20.15388166
BI-DAY 2 16:12	4	1593.2	2	Hawi substrate	-155.7946613	20.12789133
BI-DAY 2 16:26	3	1865.7	2	Hawi substrate	-155.8019344	20.14314517
BI-DAY 2 17:03	2	1630.2	3	Pololu substrate	-155.8310301	20.21652205
BI-DAY 3 09:40	4	1665.9	3	Pololu substrate	-155.8271429	20.21451058
BI-DAY 3 08:51	2	1602.3	2	Pololu substrate	-155.8286098	20.22351706
BI-DAY 3 09:02	5	1561.7	2	Pololu substrate	-155.8288735	20.22732439
BI-DAY 3 09:40	6	1665.9	3	Pololu substrate	-155.8269375	20.21424294
BI-DAY 3 10:25	2	1645.7	3	Pololu substrate	-155.8321083	20.20781667
BI-DAY 3 11:06	4	1582.8	3	Pololu substrate	-155.8132119	20.23404294
BI-DAY 3 11:56	2	1582.8	3	Pololu substrate	-155.8153648	20.23786612
BI-DAY 3 13:23	25	1461.7	3	Pololu substrate	-155.7980233	20.24810167
BI-DAY 3 13:24	27	1461.7	3	Pololu substrate	-155.7984325	20.24843742
BI-DAY 3 14:26	21	1562.3	2	Pololu substrate	-155.7985805	20.23803486
BI-DAY 3 14:28	19	1583.9	3	Pololu substrate	-155.8031599	20.2369353
BI-DAY 3 15:15	21	1590.6	3	Pololu substrate	-155.8004183	20.23522999
BI-DAY 3 16:06	6	1594.7	2	Pololu substrate	-155.7759385	20.23651331
BI-DAY 3 16:11	27	1566.6	3	Pololu substrate	-155.772855	20.24162666
BI-DAY 3 18:18	2	1607.6	2	Hawi substrate	-155.7884559	20.12265828
BI-DAY 4 06:32	2	1607.6	2	Hawi substrate	-155.7882483	20.12254856
BI-DAY 4 08:41	2	1589.3	2	Pololu substrate	-155.8357609	20.20381869
BI-DAY 4 08:44	3	1649.9	3	Pololu substrate	-155.8327098	20.20448799
BI-DAY 4 10:16	28	1694.8	3	Pololu substrate	-155.7515292	20.22112016
BI-DAY 4 10:19	20	1704.8	3	Pololu substrate	-155.7572924	20.22184944
BI-DAY 4 10:51	22	1744.1	3	Pololu substrate	-155.7644	20.22349
BI-DAY 4 10:56	17	1757.3	3	Pololu substrate	-155.7664186	20.22243042
BI-DAY 4 11:34	2	1893.7	3	Pololu substrate	-155.7860935	20.22022845
BI-DAY 4 11:36	5	1736.1	3	Pololu substrate	-155.7834318	20.22795314
BI-DAY 4 12:43	5	1801.0	3	Pololu substrate	-155.8077251	20.22032967
BI-DAY 4 12:46	2	1732.2	3	Pololu substrate	-155.8038283	20.22748634

Table 3 continued

SITE	CORRECTED LATERITE THICKNESS (M)	RAINFALL (MM/Y)	QUALITY NUMBER	COMMENT	LONGITUDE	LATITUDE
BI-DAY 4 16:29	12	1555.1	3	Pololu substrate	-155.7707587	20.24586631
BI-DAY 4 13:20	28	1603.3	3	Pololu substrate	-155.80859	20.23311332
BI-DAY 4 14:09	4	1544.6	3	Pololu substrate	-155.8300609	20.22750995
BI-DAY 4 14:50	1	1665.0	2	Pololu substrate	-155.8011533	20.23211667
BI-DAY 4 15:30	1	1675.3	2	Pololu substrate	-155.7971967	20.23129167
BI-DAY 2 09:08			1	no model	-155.84839	20.21418333
BI-DAY 2 09:17			1	no model	-155.8487501	20.21404773
BI-DAY 2 10:47			1	no model	-155.8315833	20.17405
BI-DAY 2 14:06			1	no model	-155.8393216	20.19283161
BI-DAY 3 10:21			1	no model	-155.8306746	20.20642201
BI-DAY 3 10:58			1	no model	-155.8166467	20.22455158
BI-DAY 3 11:44			1	no model	-155.8110896	20.23386709
BI-DAY 3 15:11			1	no model	-155.8014267	20.23328667
BI-DAY 4 06:38			1	no model	-155.7815316	20.12304367
BI-DAY 4 09:27			1	no model	-155.7945908	20.23206611
BI-DAY 4 09:28			1	no model	-155.7920164	20.23426656
BI-DAY 4 13:23			1	no model	-155.802295	20.23086332
BI-DAY 4 14:03			1	no model	-155.8341867	20.22719333
BI-DAY 4 14:53			1	no model	-155.8002168	20.2338529
BI-DAY 4 15:31			1	no model	-155.7994446	20.2305179
BI-DAY 4 16:28			1	no model	-155.7712502	20.24574652

Table 4. Major Element τ percent values

τ	SiO2	TiO2	Al2O3	Fe2O3	MnO	MgO	CaO	Na2O	K2O	P2O5
19-MOL-1	-59%	0%	63%	106%	-74%	-98%	-100%	-100%	-92%	-40%
19-MOL-2	-58%	0%	65%	107%	-77%	-98%	-100%	-100%	-91%	-39%
19-MOL-3	-79%	0%	-16%	138%	-40%	-93%	-98%	-100%	-90%	-5%
19-MOL-4	-79%	0%	-17%	202%	-35%	-92%	-98%	-98%	-85%	14%
19-MOL-5	-95%	0%	-91%	153%	-83%	-99%	-100%	-100%	-84%	-58%
19-MOL-6	-78%	0%	-17%	196%	-20%	-89%	-96%	-98%	-85%	52%
19-MOL-7	-96%	0%	13%	325%	-87%	-99%	-100%	-100%	-79%	6%
19-MOL-8	-95%	0%	-90%	167%	-72%	-98%	-100%	-100%	-78%	-62%
19-MOL-9	-95%	0%	-95%	75%	-77%	-99%	-100%	-99%	-87%	-78%
19-MOL-10	-97%	0%	-83%	246%	-92%	-99%	-100%	-100%	-70%	-18%
19-MOL-12	-88%	0%	-56%	214%	-52%	-95%	-98%	-95%	-75%	31%
19-MOL-14	-55%	0%	59%	137%	0%	-87%	-100%	-100%	-82%	24%
19-MOL-15	-74%	0%	72%	305%	-41%	-95%	-100%	-100%	-75%	36%
19-MOL-16	-95%	0%	-84%	182%	-81%	-98%	-100%	-100%	-74%	-49%
19-MOL-17	-55%	0%	74%	166%	-15%	-91%	-100%	-99%	-85%	-6%
19-MOL-18	-53%	0%	26%	163%	2%	-91%	-94%	-96%	-55%	77%
19-MOL-19	-50%	0%	35%	178%	67%	-94%	-95%	-87%	-6%	91%
19-MOL-20	-64%	0%	11%	211%	44%	-97%	-98%	-97%	22%	10%
19-MOL-21	-52%	0%	35%	193%	-19%	-95%	-97%	-91%	-47%	-23%
19-MOL-22	-52%	0%	40%	193%	-2%	-96%	-98%	-92%	-36%	-39%
19-MOL-23	-46%	0%	58%	197%	41%	-96%	-98%	-92%	3%	-35%
19-MOL-25	-96%	0%	-94%	170%	-75%	-98%	-100%	-100%	-80%	-43%

Table 5. Trace Element τ Analysis

τ	Ba (ppm)	Ce	Cr	Cu	Ga	La	Nb	Nd	Ni
19-MOL-1	-37%	212%	-87%	-100%	7%	411%	357%	366%	-61%
19-MOL-2	-37%	215%	-86%	-100%	8%	416%	362%	370%	-61%
19-MOL-3	-68%	253%	-90%	-99%	19%	188%	365%	344%	-89%
19-MOL-4	-75%	195%	-91%	-99%	7%	139%	253%	269%	-92%
19-MOL-5	-100%	-40%	-90%	-100%	-4%	-93%	247%	55%	
19-MOL-6	-74%	208%	-93%	-99%	14%	103%	253%	282%	-88%
19-MOL-7	-98%	72%	-77%	-100%	60%	77%	307%	261%	-79%
19-MOL-8	-100%	-20%	-88%	-100%	-8%	-69%	233%	75%	-95%
19-MOL-9	-100%	-60%	-93%	-100%	-45%	-100%	194%	-6%	-100%
19-MOL-10	-91%	259%	-81%	-100%	72%	342%	357%	382%	-93%
19-MOL-12	-83%	69%	-71%	-99%	-19%	41%	156%	143%	-92%
19-MOL-14	34%	657%	-98%	-99%	-13%	392%	223%	503%	-89%
19-MOL-15	-77%	166%	-77%	-100%	110%	52%	407%	359%	-65%
19-MOL-16	-100%	-40%	-78%	-99%	-23%	-95%	151%	52%	-99%
19-MOL-17	-41%	406%	-85%	-100%	18%	284%	380%	403%	-69%
19-MOL-18	46%	551%	-94%	-84%	-1%	417%	289%	563%	-87%
19-MOL-19	149%	373%	-79%	-90%	-7%	270%	228%	395%	-78%
19-MOL-20	9%	169%	-36%	-67%	17%	76%	187%	264%	-64%
19-MOL-21	15%	513%	-67%	-94%	8%	469%	296%	499%	-78%
19-MOL-22	-8%	352%	-59%	-95%	6%	232%	289%	395%	-73%
19-MOL-23	41%	504%	-69%	-94%	11%	416%	316%	549%	-69%
19-MOL-25	-100%	-54%	-80%	-99%	0%	-100%	186%	43%	-100%

Table 5 continued

τ	RB	SC	SM	SR	TH	V	Y	ZN	ZR	PB	U
19-MOL-1	-49%	-96%	111%	-62%	1196%	-71%	-84%	-49%	568%	-70%	314%
19-MOL-2	-49%	-96%	114%	-61%	1209%	-71%	-84%	-48%	574%	-65%	125%
19-MOL-3	-43%	-94%	161%	-91%	860%	-60%	-64%	-23%	373%	-63%	161%
19-MOL-4	-48%	-95%	124%	-91%	701%	-63%	-72%	-39%	315%	-91%	53%
19-MOL-5	-50%	-100%	13%	-97%	546%	-60%	-91%	-85%	144%	-56%	136%
19-MOL-6	-39%	-93%	137%	-93%	733%	-58%	-64%	-19%	314%	-91%	191%
19-MOL-7	-24%	-100%	123%	-96%	1408%	-45%	-88%	-82%	418%	-86%	36%
19-MOL-8	-35%	-100%	23%	-97%	452%	-66%	-90%	-73%	143%	-89%	11%
19-MOL-9	-64%	-100%	-35%	-98%	220%	-71%	-90%	-86%	40%	-96%	126%
19-MOL-10	-2%	-100%	183%	-91%	1410%	-32%	-81%	-89%	453%	-77%	92%
19-MOL-12	-53%	-100%	53%	-89%	450%	-63%	-85%	-64%	181%	-30%	189%
19-MOL-14	-17%	-77%	274%	-87%	687%	-66%	-69%	15%	354%	-66%	209%
19-MOL-15	25%	-100%	207%	-96%	2112%	-42%	-77%	-25%	545%	-87%	-9%
19-MOL-16	-22%	-100%	11%	-98%	355%	-51%	-90%	-80%	35%	-47%	398%
19-MOL-17	-24%	-94%	204%	-89%	1323%	-66%	-80%	-4%	749%	46%	129%
19-MOL-18	22%	-83%	266%	-64%	595%	-63%	-39%	177%	315%	-20%	148%
19-MOL-19	186%	-89%	197%	-2%	448%	-66%	-16%	21%	256%	-55%	102%
19-MOL-20	387%	-82%	130%	-64%	594%	-35%	-22%	-25%	218%	-44%	187%
19-MOL-21	67%	-81%	243%	-64%	603%	-62%	-56%	-10%	337%	-43%	169%
19-MOL-22	141%	-69%	194%	-73%	709%	-55%	-24%	-7%	320%	-36%	182%
19-MOL-23	306%	-69%	264%	-63%	823%	-55%	37%	8%	351%	-81%	13%
19-MOL-25	-42%	-100%	10%	-98%	412%	-51%	-91%	-76%	95%	-84%	33%

Table 6. Water chemistry for wells and groundwater sites on Molokai.

Sample Site	pH	Conductivity (uS/cm)	Major Cations (mg/L)				Major Anions (mg/L)			
			$Ca^{2}+$	$Mg^{2}+$	Na+	K+	HCO_3-	Cl-	SO_4^{2}-	SiO_2
USGS 210638157032601 4-0603-01 D14 Umipaa, Molokai, HI	7.7	2400.0	57.0	55.0	320.0	28.0	214.0	650.0	63.0	53.0
USGS 211012157041801 MOLOKAI IRRIGATION OFFICE AT HOOLEHUA, MOLOKAI	7.4	320.0	9.6	12.0	29.0	2.8	40.0	65.0	13.0	39.0
USGS 210857156010701 4-0801-02 Kauluwai 2, Molokai, HI			12.0	15.0	30.0	3.1		76.0	21.0	43.0
USGS 210856157011201 4-0801-01 Kauluwai 1 (W16), Molokai, HI	8.0	310.0	8.8	9.7	30.0	2.8	48.0	58.0	13.0	44.0
USGS 210857157011701 4-0801-03 Kualapuu Mauka, Molokai, HI	8.2		9.6	11.0	33.0	3.0		64.0	11.0	46.0
USGS 210903157013001 4-0901-01 Kalualohe W17, Molokai, HI	8.0	260.0	7.8	8.0	21.0	2.8	45.0	60.0	7.1	47.0
USGS 210850156552201 4-0855-06 Waikolu 4, Molokai, HI	8.1		6.6	3.3	9.0	1.4		11.0	2.0	33.0
USGS 210605157012001 4-0601-01 Kaunakakai W11, Molokai, HI	7.2	270.0	13.0	11.0	25.0	1.7	112.0	30.0	5.1	28.0
USGS 210711157000501 4-0700-01 Kakalahale, Molokai, HI	7.6	1705.0	20.5	35.0	240.0	14.5	44.0	465.0	53.5	48.0
USGS 211040156580401 4-1058-01 National Park, Kalaupapa, Molokai, HI	7.7	180.0	8.3	5.3	15.0	1.9		20.3	3.3	21.3
USGS 210419156570501 4-0457-01 Kawela Shaft (S4), Molokai, HI	6.3	380.0	13.0	11.0	38.0	3.6		82.0	12.0	32.0
USGS 210402156495801 4-0449-01 Ualapue Shaft (S6), Molokai, HI	7.3	420.5	12.6	9.9	56.0	4.4	96.0	74.0	12.9	45.0

Table 7. XRD results Molokai soil samples

SAMPLE	GOETHITE (%)	HEMATITE (%)	GIBBSITE (%)	KAOLINITE (%)	QUARTZ (%)	MAGHEMITE (%)	2:1 CLAY (%)	PLAGIOCLASE (%)	MG-CALCITE (%)	FERRIHYDRITE (%)	AMORPHOUS (%)
19-MOL-1	21.05	18.67	15.85	6.16	5.81	32.47					
19-MOL-1 (DISC 2)	21.05	18.67	15.85	6.16	5.81	32.47					
19-MOL-2	23.84	11.22	8.26	29.96	6.73	19.99					
19-MOL-3	23.87	8.71	53.50	6.25	1.74	5.93					
19-MOL-4	45.85	32.06	12.99	0.37	8.34	0.40					
19-MOL-5	9.29	12.95	29.96	22.00	11.95	11.42			2.43		
19-MOL-6	32.98	2.27	14.01	8.47	11.12	0.61	31.15				
19-MOL-7	43.44	28.59	3.93	0.10	6.29	0.70	17.66				
19-MOL-8	21.45	15.46	17.97	36.03	4.70	4.38					
19-MOL-9	23.47	18.76	24.94	21.40	9.07	2.36					
19-MOL-10	25.97	7.57	2.85	52.32	5.00	6.28					
19-MOL-11						2.18	11.00			5.81	81.00
19-MOL-12	15.78	10.30	1.54	26.23	1.40	19.28	25.47				
19-MOL-14	8.44	5.85	10.33	28.41	7.17	1.98	37.82				
19-MOL-15	65.11	18.38	9.46	2.13	1.68	3.24					
19-MOL-16	12.26	14.32	0.94	40.56	7.93	24.00					
19-MOL-17	30.19	6.84	11.60	34.78	7.20	9.39					
19-MOL-18	1.69	9.57	16.50	52.27	3.04	9.98		6.96			
19-MOL-19	5.00	20.30	24.56	31.67	0.57	17.91					
19-MOL-20	18.70	13.22	7.96	42.02	4.90	13.19					
19-MOL-21	8.77	21.33	1.06	42.88	1.33	18.15	6.48				
19-MOL-22	9.43	21.78	5.53	44.88	5.03	13.35					
19-MOL-23	14.83	43.52	18.77	10.90	5.49	6.50					
19-MOL-24	6.23	13.41	0.00	57.11	0.00	12.05		11.20			
19-MOL-25	23.25	41.04	7.06	2.10	19.26	7.29					